

# LIQUEFACTION MITIGATION WITH DEEP MIXING

Ross W. Boulanger, University of California, Davis, California, USA, [rwoulanger@ucdavis.edu](mailto:rwoulanger@ucdavis.edu)  
Lisheng Shao, Keller North America, Inc., Santa Paula, California, USA, [LShao@Keller-na.com](mailto:LShao@Keller-na.com)

## ABSTRACT

Deep mixing methods have been used to mitigate the effects of earthquake-induced liquefaction for a wide range of civil infrastructure, including buildings, bridges, ports, transportation systems, levees, and embankment dams. Soil-cement reinforcements can reduce the potential for triggering of liquefaction, reduce lateral and vertical ground deformations, and provide support for overlying structures. Soil-cement columns, walls, and grids constructed by deep mixing or other methods can be an effective option for treating soil deposits that include strata of silty and clayey soils that are generally difficult to improve by densification techniques. General design considerations are summarized followed by detailed discussion of different treatment mechanisms and associated design challenges. Results from a dynamic centrifuge model test and associated nonlinear dynamic analyses for an embankment on liquefiable soils treated with soil-cement walls are presented and used to illustrate several challenges. The application of deep mixing to mitigate against liquefaction at the abutments of the West Dowling Road Overcrossing and the subsequent good performance of this bridge during the 2018  $M_w=7.1$  Anchorage Earthquake are described. Concluding remarks and discussion of future needs are presented.

**Keywords:** liquefaction, deep mixing, grids, columns, case history

## INTRODUCTION

Deep mixing (DM) methods have been widely used to mitigate the effects of earthquake-induced liquefaction for a range of civil infrastructure, including buildings, bridges, ports, transportation systems, levees, and embankment dams (Bruce 2001, Moseley and Kirsch 2004, Kitazume and Terashi 2013). Soil-cement columns, walls, and grids constructed by deep mixing (Fig. 1) or other methods are often an effective option for liquefaction mitigation when the subsurface soils are difficult to improve by densification techniques, such as may be the case with finer grained soils like sandy silt, silt, or clayey silt.

Case histories have demonstrated that sites treated by DM methods have generally performed well in past earthquakes. Cases from the 1995 Kobe Earthquake include the good performance of a grid system protecting the pile foundations for a 14-story building on a waterfront pier (Suzuki et al. 1996, Tokimatsu et al. 1996). Tokunaga et al. (2015) surveyed member companies of the CDM Association regarding performance of structures with DM treatments during the 2011 Tohoku earthquake, including river embankments, levees, seawalls, road embankments, and building foundations. The survey replies identified 789 structures with sufficient field data to classify them as not damaged, plus another 58 structures without reported damage that were nonetheless classified as unknown or unclear because of limitations in the field survey data (e.g., inaccessibility for inspections) at that time. Several case histories were described in detail to illustrate the good performance of treated areas relative to adjacent untreated areas, demonstrating the effectiveness of the treatments. Detailed analyses for specific case histories have shown that the good performance of DM treated areas can be reasonably predicted using currently available analysis methods (e.g., Yamashita et al. 2018). These and other case histories (e.g., Martin et al. 2004, Kitazume 2016, Christie et al. 2019) have provided invaluable lessons on various aspects of DM treatments, from construction to performance during earthquakes.

The complexity of mechanisms involved in DM treatments of liquefiable soils can pose a challenge for designers, often leading to additional conservatism in design practices. Design analysis methods can

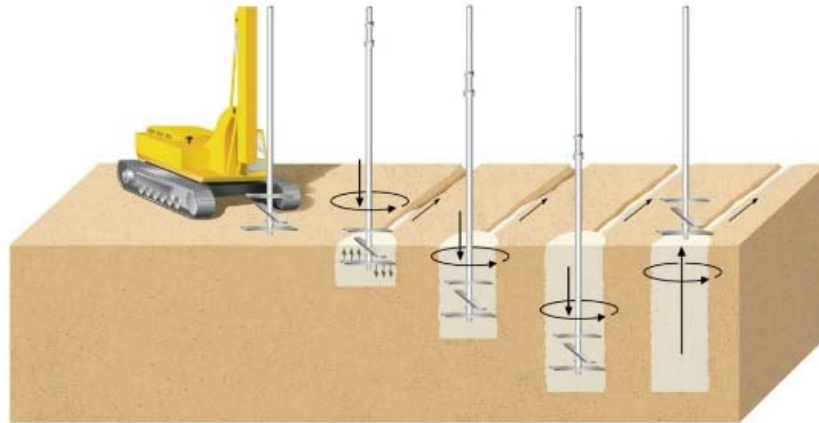


**Fig. 1. Schematic of deep mixing using a single-shaft mixing machine (courtesy of Keller)**

range from simplified equivalent-static methods to complex three-dimensional (3D) dynamic methods, depending on the project-specific constraints. The complex geometry of an infrastructure system and its DM treatment configuration, combined with the highly nonlinear responses of liquefiable soils and soil-cement materials, can be difficult to approximate with any analysis method, whether simplified or complex. The final design can be significantly affected by uncertainties associated with the predicted performance, such that research on fundamental mechanisms and design procedures continue to be needed as one part of advancing the effective use of this technology in practice.

In this paper, select issues regarding the use of DM for liquefaction mitigation are reviewed and discussed. General considerations in the design of DM treatments are summarized, including alternative DM configurations, treatment mechanisms, failure modes, liquefiable soil characterizations, ground motions, performance objectives, analysis methods, and design challenges. The treatment mechanisms and select design challenges are examined in more detail, including aspects of the soil-cement properties, prevention of liquefaction triggering using DM column or grid arrangements, reduction of lateral spreading or ground deformations, and protection of overlying structures. Results from a dynamic centrifuge model test and associated nonlinear dynamic analyses (NDA) for an embankment on liquefiable soils treated with soil-cement walls are presented and used to illustrate various challenges. The application of deep mixing to mitigate against liquefaction at the abutments of the West Dowling Road Overcrossing and the subsequent performance of this bridge during the 2018  $M_w=7.1$  Anchorage Earthquake are described. Concluding remarks and discussion of future needs are presented.

## **GENERAL DESIGN CONSIDERATIONS**

Procedures for designing DM ground improvements are generally more established for static loading conditions than for seismic loading conditions involving liquefaction. Nonetheless, design guidance for various configurations and loading conditions, including for liquefaction mitigation, can be found in JGS (1998), PWRI (1999), Topolnicki (2004), Kitazume and Terashi (2013), Bruce et al. (2013), and Kitazume (2016). These guidance documents address aspects of constructability, quality control, properties, analysis methods, internal and global failure mechanisms, and other aspects important to static or seismic design. Design for liquefaction remediation depends on numerous project-specific factors, including the system's configuration, site conditions, seismic hazard, performance objectives, project risks, constructability, and supporting experiences. Design practices for addressing each of these factors can vary regionally and across industry segments, such that it is necessary to approach problems from first principles in many situations.

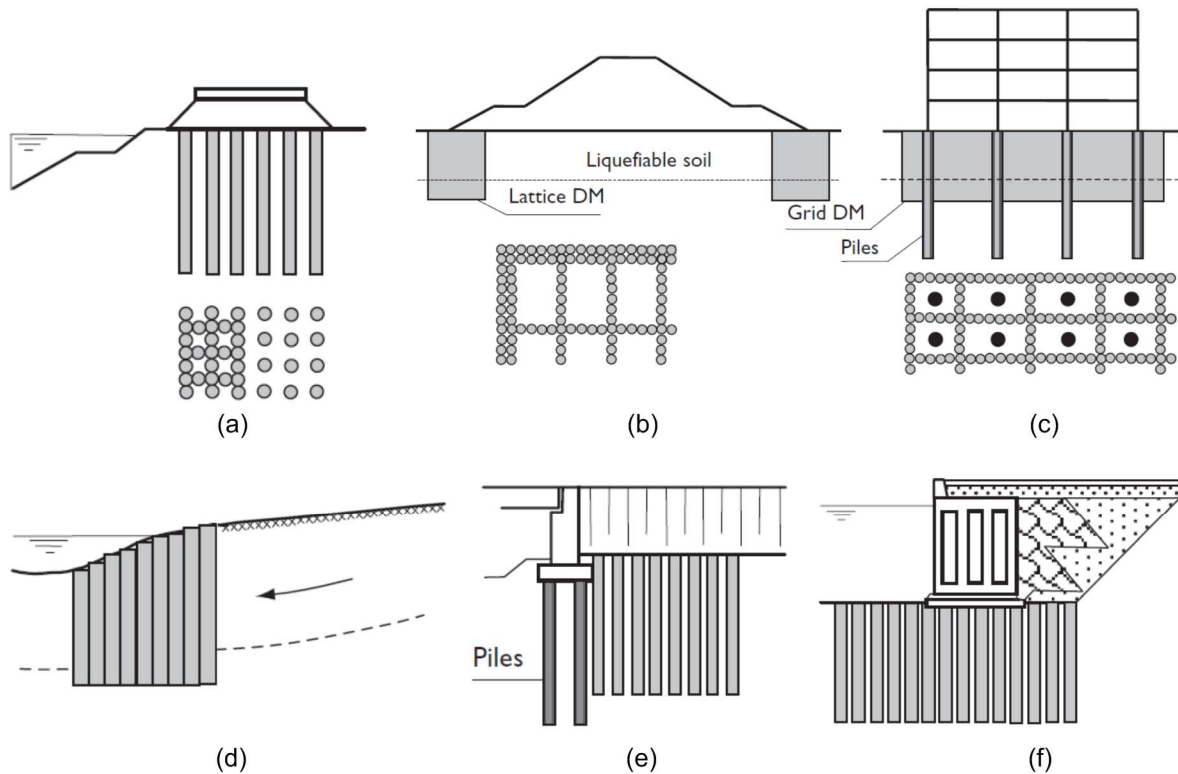


**Fig. 2. Examples of deep mixing applications and patterns: (a) road embankment, (b) levee or dam, (c) pile foundation, (d) lateral spreading buttress, (e) bridge abutment, and (f) quay wall (Topolnicki 2004)**

A wide range of DM treatment configurations have been used for different infrastructure systems, schematically illustrated in Fig. 2 (Topolnicki 2004). DM can be used to construct columns with variable spacing (Fig. 2a), walls or panels that can be arranged in grids or lattices (Fig. 2b,c), solid blocks, or a composite arrangement of columns, grids, and blocks (Fig. 2a). DM treatments may be used to support structures in areas of approximately level ground (Fig. 2c), restrain slopes or embankments against lateral deformations (Fig. 2a,b,d), or support structures and protect them against lateral ground deformations (Fig. 2e,f). In cases where permanent lateral ground movements are unlikely to be large (e.g., level ground, Fig. 2c), the design still needs to consider transient lurching of the liquefied ground during shaking. In cases where permanent lateral ground deformations are likely to be larger than acceptable without DM treatments (e.g., any case involving significant slopes or nearby free faces), the design needs to consider how DM treatments can be configured to reduce expected deformations to acceptable levels.

Jet Grouting uses high velocity fluid jets to erode and mix the in-situ soil with grout to form soilcrete. Although the jet grouting installation method is different from deep mixing, the material properties of the jet grouting final product are similar to those for deep mixing. Jet grouting is versatile and can accommodate difficult site restrictions, such as existing footings, underground obstructions, or limited overhead spaces. Jet grouting can form soil-cement columns, grids, and blocks for different infrastructure systems and be used for liquefaction mitigations. The analysis methods and considerations discussed herein for DM are generally also applicable for jet grouting treatments.

The mechanisms by which DM treatments mitigate liquefaction effects may be generally grouped in the following five categories.

- Admixture stabilization: The mixing of binders with liquefiable or weak soil produces a soil-cement with increased strength and stiffness. Full replacement of liquefiable soils by DM treatment eliminates liquefaction as a concern, whereas partial replacement mitigates against liquefaction effects through other mechanisms.
- Prevention of liquefaction triggering: DM inclusions can stiffen the soil profile, thereby reducing the shear strain imposed on the enclosed native soils and slowing the generation of excess pore water pressures. Sufficient stiffening can prevent liquefaction triggering, which helps prevent ground deformations or settlements from becoming unacceptably large.
- Control of lateral ground deformations: The lateral and vertical shear resistance of the DM inclusions can reduce local or global deformations within or adjacent to the treatment zone, even if the soils between the inclusions liquefy during strong shaking.
- Control of pore pressure migration: Continuous DM walls of lower-permeability can impede lateral diffusion of excess pore pressures, thereby preventing high excess pore pressures in adjacent untreated liquefied areas from migrating laterally into the non-liquefied soils of the DM treated area.
- Support and protection of overlying structures: DM inclusions can provide vertical load carrying capacity (support) for overlying structures, even if the soils between the DM inclusions liquefy. DM inclusions can also protect overlying structures and deep foundations from the detrimental effects of lateral ground deformations.

The above mechanisms of improvement depend on the properties of the DM materials and their potential for cracking or post-peak strain softening, as well as on the properties of the native soils. The construction of DM elements generally does not improve (e.g., densify) the adjacent native soils and the DM elements do not provide increased drainage during earthquake loading given their generally low permeability. The relative role of each treatment mechanism depends on the given application and loading conditions.

The characterization of liquefiable and non-liquefiable strata at a site can have significant effects on the design and cost of DM treatments. A certain level of site characterization work may be sufficient for identifying whether a liquefaction problem exists, but additional characterization work can be beneficial for design of the ground improvements, depending on the scale of the project. The additional characterization may address issues related to the extent of problem soils, the properties of the problem soils, and the properties of any soils affecting constructability (Bruce et al. 2013). The original conclusion that a liquefaction problem exists may itself warrant reexamination if the original evaluation was notably conservative, the site characterization data has significant limitations (e.g., non-standard drilling or penetration testing, worn equipment, inadequate calibrations), or the problem soils are difficult to characterize (e.g., thinly interbedded sands, silts, and clays; intermediate soils; soils with large particles). These issues are beyond the scope of this paper, so the reader is referred elsewhere for guidance regarding site characterization and liquefaction evaluations (e.g., Idriss and Boulanger 2008) and discussions of knowledge gaps and challenges in liquefaction evaluations (e.g., Bray et al. 2017, Boulanger et al. 2019).

The seismic ground motions that develop at a site are affected by any DM improvements, such that the remediation of liquefaction can sometimes increase the seismic force and displacement demands imposed on an overlying structure relative to those expected if the soils were allowed to liquefy. However, it is also common in design practice to check that an overlying structure can resist the seismic demands that would develop in the absence of liquefaction; i.e., the reduction in seismic demand on a superstructure due to liquefaction in the subsurface is usually not relied on. The effect of DM improvements on seismic response may be evaluated indirectly based on the estimated equivalent shear stiffness of the treated ground or directly using a nonlinear dynamic analysis method.

Analysis methods for designing DM improvements can range from simplified equivalent-static methods to complex two-dimensional (2D) or three-dimensional (3D) nonlinear dynamic methods, depending on

project-specific constraints. The nature of the analysis model depends on the infrastructure system and the anticipated deformation and damage modes that the analysis model will need to approximate. Two-dimensional analysis methods generally rely on homogenization of treatment zones (i.e., composite properties). Three-dimensional models can more realistically represent complex DM geometries, but generally require greater engineering effort and the options for soil constitutive models may be more limited depending on the software platform. The tradeoff between engineering effort and analysis model complexity depends on what features of behavior are most important to the design, how the design work may impact the schedule and budget, and the potential construction cost savings. Regardless, the limitations in any analysis method need to be recognized and accounted for, including aspects related to progressive damage, cracking, and localizations in DM materials, the cyclic stress-strain responses of liquefiable soils, and the diffusion of excess pore pressures. Sensitivity analyses that account for various sources of uncertainty and modeling limitations are generally used to provide bounds on the expected performance.

Performance objectives for the infrastructure being protected by the DM improvements should be clearly established, particularly regarding acceptable levels of damage at different hazard levels. Acceptable damage levels for any building (e.g., ASCE 7-16) or infrastructure system also dictate the acceptable range of strains or stresses imposed on DM materials during seismic loading. For example, if the objective is to maintain full operability of an important building facility for the design earthquake loading, it may be necessary to limit ground settlements to relatively small levels and, consequently, either prevent liquefaction triggering or limit the extent of nonlinearity that is expected in the DM materials. In contrast, if the objective is to prevent uncontrolled release of a reservoir behind a zoned embankment with ample freeboard, it may be possible to accept considerably larger deformations, such that extensive damage to the DM materials during the design earthquake loading may be acceptable. The cost of DM improvements can be significantly affected by the performance objectives, such that the relative cost of achieving different levels of performance may be evaluated as part of the design process.

## MECHANISMS AND ISSUES FOR LIQUEFACTION MITIGATION

The relative roles of different DM treatment mechanisms are project specific, as noted previously. The designer must consider internal and global stability and deformation mechanisms for static or dynamic loading that vary with the specific application (e.g., Kitazume and Terashi 2013, Bruce et al. 2013). The following subsections are limited to a subset of issues: soil-cement properties, preventing liquefaction triggering using columns, preventing liquefaction triggering using grids, reducing lateral spreading and embankment displacements, and supporting or protecting overlying structures.

### *Soil-cement properties*

Design shear strengths for DM soil-cement improvements under static loading conditions may be estimated from the results of unconfined compression strength tests with appropriate modifications for field conditions (Bruce et al. 2013) as,

$$s_{dm} = \frac{1}{2} q_{dm,spec} f_r f_c f_v \quad [1]$$

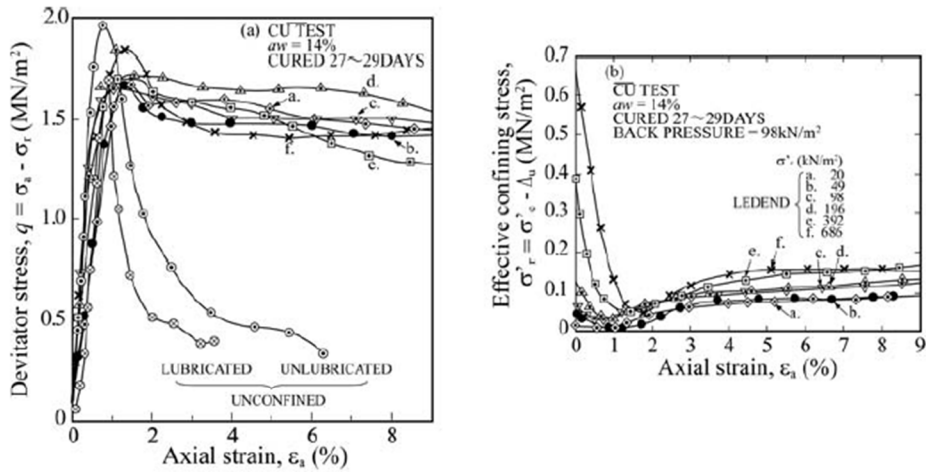
where  $s_{dm}$  = shear strength (i.e., used with friction angle  $\phi = 0$ ) for the DM materials,  $q_{dm,spec}$  = unconfined compressive strength ( $q_u$ ) as specified for field conditions,  $f_r$  = ratio of the confined large-strain shear strength to the peak unconfined compressive strength,  $f_c$  = curing factor to account for in-situ strength gains over time, and  $f_v$  = factor to account for spatial variability in the in-situ shear strength. Each of the adjustment factors are discussed in this section.

The  $q_u$  for field conditions may be less than for laboratory mixed specimens because of differences in the specimen uniformity, curing conditions, or other factors, although the reverse situation has been observed for some projects. Kitazume and Terashi (2013) summarized Japanese experiences showing that strengths from field core samples could be as low as 1/2 to 1/3 of the strengths from laboratory prepared specimens for on-land construction in clay deposits, or as low as 1/2 the laboratory strengths for on-land construction in sand deposits. Bruce et al. (2013) report that a common expectation in US practice is for field strengths to exceed 50% of the strengths for laboratory mixed specimens, but that experience on other projects with similar equipment and soils should be considered in estimating this ratio during design.

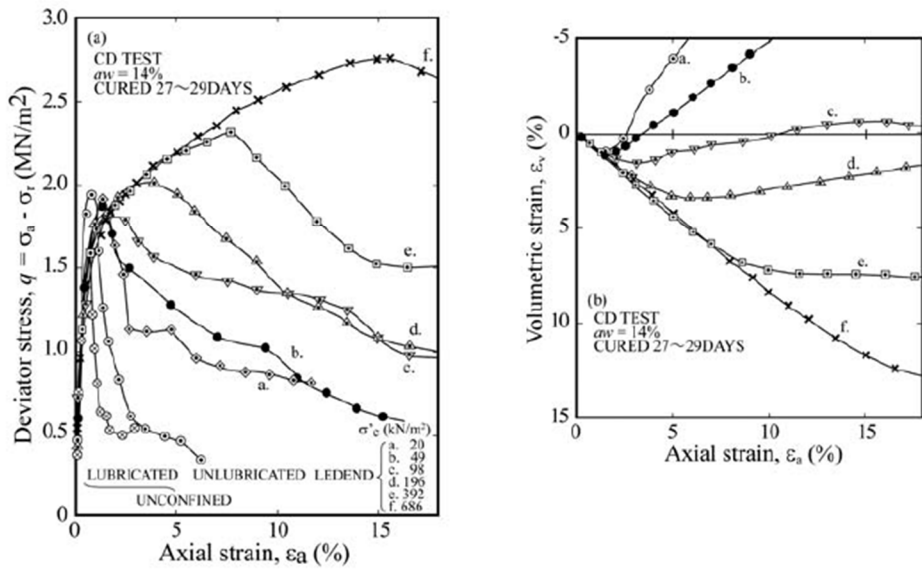
The shear resistance of soil-cement is usually brittle for unconfined conditions, but becomes relatively ductile with modest amounts of confining stress. Tatsuoka and Kobayashi (1983) showed that large-strain compressive strengths in undrained triaxial compression tests were about 80% of the  $q_u$  for a cement-treated clay with a  $q_u$  of about 2.0 MPa (Fig. 3a). The same authors showed that large-strain shear resistances in drained triaxial compression tests also became increasingly ductile with increasing confining stress, although the effect was more gradual than for undrained loading (Fig. 3b). Terashi et al. (1980) showed that the large-strain compressive strengths in unconsolidated undrained triaxial compression tests with relatively modest confining stresses were about 50–80% of the  $q_u$  for quicklime-treated clay with a  $q_u$  of 0.6–1.3 MPa (Fig. 4). Other researchers have reported similar findings for tests on other cement-treated soils (e.g., Yu et al. 1997, Coastal 2002, Quiroga et al. 2015) or plastic concretes (e.g., Mahboubi and Ajorloo 2005). To account for the progressive failure that can develop in soil-cement components due to post-peak strain-softening behavior, Kitazume et al. (2000) used 80% of  $q_u$  (i.e.,  $f_r = 0.8$ ) in their limit equilibrium analyses of centrifuge model tests of caissons supported on soil-cement columns in soft clay.

The curing factor can be estimated from empirical relationships, but should be confirmed or revised based on mix design testing data. The curing factor expression in Bruce et al. (2013) suggests that strengths can be conservatively estimated to increase by a factor of 1.5 from 28 days to 1 year (i.e.,  $f_c = 1.5$  if  $q_{dm,spec}$  is based on 28 day strengths) or by a factor of 1.8 from 28 days to 5 years. Selection of design curing factors should consider the expected timing of design load applications. For example, a smaller  $f_c$  may be appropriate for static design loads that will be applied within a few months of DM completion, whereas a larger  $f_c$  may be appropriate for seismic loads having a low probability of occurrence within the first year or so of DM curing.

Spatial variability factors for deterministic analyses of DM treatments are presented in Bruce et al. (2013) using the statistical analysis approach described in Filz and Navin (2010). The objective of this statistical analysis approach was to have the same probability that actual shear strengths exceed actual shear stresses in both the soil-cement and untreated soil portions of a potential failure surface in a limit equilibrium analysis. The approach considered five factors: (1) the probability that actual soil strength exceeds the design soil strength,  $p_s$ , (2) the coefficient of variation in soil strength,  $V_s$ , (3) the probability that actual DM soil-cement strength exceeds the specified DM soil-cement strength,  $p_{dm}$ , (4) the coefficient of variation in the DM soil-cement strength,  $V_{dm}$ , and (5) the design value for the limit equilibrium factor of safety,  $F_d$ . Bruce et al. (2013) used this approach to produce  $f_v$  values ranging from 0.58 to 1.25 for a range of assumptions regarding the above parameters ( $p_s$  of 0.67,  $V_s$  of 0.25,  $p_{dm}$  of 0.7–0.9,  $V_{dm}$  of 0.4–0.6,  $F_d$  of 1.2–1.6). Values of  $f_v$  greater than unity are possible because  $V_{dm}$  is generally greater than  $V_s$  and  $p_{dm}$  is generally greater than  $p_s$ . Values of  $f_v$  increased with increasing  $p_{dm}$  and decreasing  $F_d$ , with the recommended  $f_v$  values being approximately equal to or greater than 1.0 for cases with  $p_{dm} \geq 0.8$ , and  $F_d = 1.2$ . Thus, an  $f_v$  value of about unity may be appropriate for seismic applications that allow significant yielding (e.g.,  $F_d = 1.0$  when determining a pseudo-static yield acceleration) and involve relatively large global deformation mechanisms (e.g., the average shear resistance over a larger volume or area will have a smaller coefficient of variation; Baecher and Christian 2003).



(a) Consolidated undrained shear tests.



(b) Consolidated drained shear tests.

**Fig. 3. Triaxial compression tests on cement-stabilized soil with different confining stresses (Tatsuoka and Kobayashi 1983; from Kitazume and Terashi 2013)**

The Young's modulus ( $E$ ) has been shown to be approximately proportional to  $q_u$  and relatively independent of confining stress for DM soil-cements. Niina et al. (1981), as reported in Kitazume and Terashi (2013), summarized data for 16 cement-treated clays and sandy silts showing that the secant value of the Young's modulus at a deviator stress equal to half the  $q_u$  (i.e.,  $E_{50}$ ) ranged from 350–1,000 times  $q_u$ . Navin and Filz (2006) reported that the  $E_{50}/q_u$  ratio was about 300 for a large dataset for tests from wet-mixed columns. Various studies, as summarized in Porbaha et al. (2000), have reported  $E_{50}/q_u$  ratios ranging from 50–1,000. Bruce et al. (2013) noted that modulus measurements are strongly affected by compliance in the equipment and end platens (unless local strain measurements on the specimens are used) and creep effects, and subsequently suggested that  $E_{50}/q_u$  could be estimated for design as 150 for dry mixing or 300 for wet mixing. Filz et al. (2015) summarized data from a project involving deep mixing by the wet method, wherein the test data suggested  $E_{50}/q_u$  was about 625 from local strain measurements versus about 300 from end-platen measurements. For seismic evaluations, the selection of a smaller  $E_{50}/q_u$  may or may not be conservative depending on the characteristics of the soil or soil-

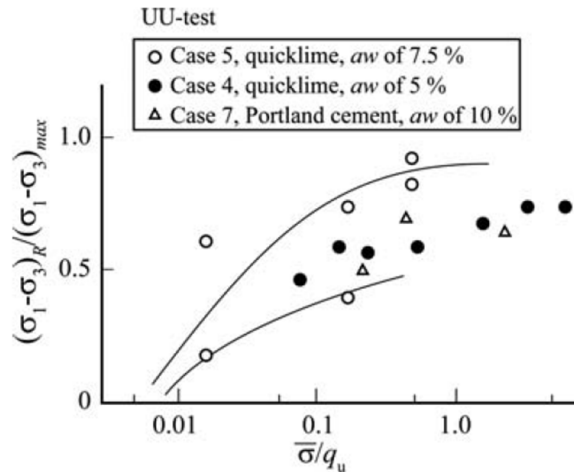


**Fig. 4. Ratio of large-strain (residual) shear resistance to peak shear resistance in UU triaxial compression tests versus the triaxial confining stress normalized by the unconfined compressive strength ( $q_u$ ) for quicklime-treated clays with  $q_u$  of 0.6 to 1.3 MPa (Terashi et al. 1980; from Kitazume and Terashi 2013)**

structure system being evaluated. For liquefaction remediation projects, it is suggested that sensitivity to system stiffness be considered in design, and that an  $E_{50}/q_u$  range of 300–600 in combination with expected values for the median  $q_u$  would be reasonable for this purpose.

#### ***Preventing liquefaction triggering – Columns***

The prevention of liquefaction triggering can be one objective of using DM columns, with the expectation that ground deformations are likely to be acceptably small if liquefaction of the native soils around the DM columns is precluded. The effectiveness of DM columns for preventing liquefaction triggering can be expected to depend on the properties of the columns (e.g., flexural stiffness, boundary restraints, diameter, length, spacing), the characteristics of the liquefiable strata (e.g., liquefiable soil thickness, cyclic strength, relative density), the initial static loading conditions (e.g., water table depth, superstructure loads), and ground motion characteristics (e.g., frequency content, intensity). The effectiveness of DM columns may be evaluated using a unit cell analysis method if the foundation area is relatively large and the ground surface is approximately level.

The design assumption of shear strain compatibility between the native soil and DM columns has been applied to a range of DM configurations as a means for estimating the reduction in seismic shear stresses imposed on the native soil. The assumption of shear strain compatibility was proposed by Baez (1995) for vibro-displacement stone columns where shear moduli are only several times those of the native soil, and later extended by others to soil-cement treatments that are much stiffer (e.g., Durgunoglu 2006). However, shear strains in the native soil and DM columns can be expected to become increasingly incompatible as the contrast in their shear moduli increases.

Various researchers have demonstrated that flexure and rotation of discrete columns reduces their effectiveness for reducing the seismic shear stresses on the native soil, relative to that predicted based on shear strain compatibility. Goughnour and Pestana (1998) examined the mechanical response of an elastic column in elastic soil using analytical expressions and concluded that the columns would not significantly reduce shear stresses in the soil for the column length-to-diameter ratios typically encountered in practice. Olgun and Martin (2008a,b) examined the relative contributions of shear and flexure in columns using

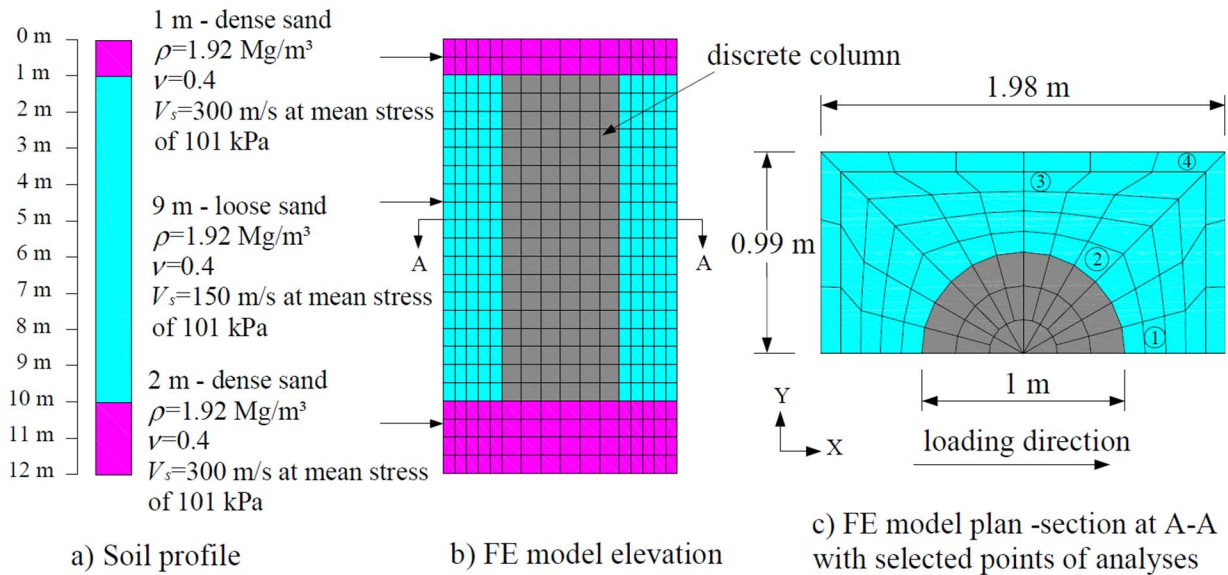


**Fig. 5. Finite element model for a unit cell from a periodic arrangement of columns through a liquefiable layer with overlying and underlying dense sands (Rayamajhi et al. 2014)**

3D dynamic FE modeling with linear elastic and nonlinear constitutive models and showed that the columns did not significantly reduce seismic shear stresses in the native soil. Green et al. (2008) performed 2D plane-strain analyses of an elastic "column" (or wall) in elastic soil, and showed that the column deformed in a combination of flexure and shear, with the role of flexure being greater near the ground surface. Bouckovalas et al. (2006) and Papadimitriou et al. (2006) examined the dynamic site response of columnar reinforced soil deposits using one-dimensional (1D), 2D, and 3D analysis models, and showed that the equivalent shear stiffness of the treated profile would be greatly overestimated by the assumption of shear strain compatibility.

Rayamajhi et al. (2014) performed linear-elastic 3D dynamic analyses to develop a relationship describing the average shear stress reduction on soil between periodic column reinforcements. The analyses considered a unit cell for a soil profile comprised of a 1-m thick compacted sand layer, over a 9-m thick liquefiable layer, over a 2-m thick dense sand layer (Fig. 5). Elastic moduli varied with the square root of vertical stress for all three layers, with the overlying and underlying dense sand layers being four times stiffer than the liquefiable layer for the same vertical stress. The columns extended from the bottom to the top of the liquefiable layer, such that the column length ( $L$ ) was always 9 m. The analyses examined a broad range of area replacement ratios ( $A_r = A_c/A_t$ , where  $A_c$  = column area,  $A_t$  = total area) and shear modulus ratios ( $G_r = G_c/G_s$ ,  $G_c$  = shear modulus of the column material,  $G_s$  = shear modulus of the liquefiable soil). Column diameters ( $D$ ) of 0.3, 0.6, 1.0, and 2.0 m were used, which correspond to  $L/D$  of 4.5, 9, 15, and 30. The analyses included pseudo-static loading and dynamic loading using harmonic input motions and earthquake ground motions.

Rayamajhi et al.'s (2014) analysis results showed that the distribution of shear stresses between the columns and native soil was affected by the  $L/D$  ratio, location within the treatment interval, and frequency content of the input motion, but that these effects were of secondary importance. Overall, the effect of the columns on the average cyclic stress ratio (CSR) imposed on the soil was expressed as,

$$R_{CSR} = \frac{CSR_I}{CSR_U} = \frac{(a_{\max} r_d)_I}{(a_{\max} r_d)_U} = R_{a_{\max}} R_{r_d} \quad [2]$$

where  $CSR_U$  = the cyclic stress ratio on the soil for the unimproved case,  $CSR_I$  = the cyclic stress ratio on the soil between the columns for the improved case,  $a_{\max,U}$  = maximum horizontal ground acceleration for the unimproved case,  $a_{\max,I}$  = maximum horizontal ground acceleration for the improved case,  $r_{d,U}$  = shear stress coefficient for the unimproved case,  $r_{d,I}$  = shear stress coefficient for the improved case,  $R_{a_{\max}}$  = ratio of the maximum surface acceleration for the improved case versus the unimproved case, and  $R_{r_d}$  = ratio of the shear stress coefficient for the improved case versus the unimproved case (referred to as the shear stress reduction factor). The above expression explicitly separates the two primary effects of the reinforcing columns: the effect on dynamic site response, which largely determines the average dynamic shear stresses, and the effect on how the average dynamic shear stresses are shared between the soil and columns. The shear stress reduction factor, as obtained from the finite element analyses, was reasonably approximated by the following expressions,

$$R_{r_d} = \frac{1}{G_r \left[ A_r \gamma_r C_G + \frac{1}{G_r} (1 - A_r) \right]} \leq 1.0 \quad \text{with } G_r \leq 30 \quad [3]$$

$$\gamma_r = 1.04 (G_r)^{-0.65} - 0.04 \quad [4]$$

where  $\gamma_r$  = ratio of the shear strain in the columns ( $\gamma_c$ ) versus in the soil between the columns ( $\gamma_s$ ), and  $C_G$  = equivalent shear factor, which depends on the inclusion's cross-sectional geometry. For  $G_r > 30$ , the columns are sufficiently rigid relative to the soil such that shear deformation of the treated ground is accommodated primarily by racking of the columns, with further increases in  $G_r$  not significantly reducing soil shear stresses. For this reason,  $R_{r_d}$  should be computed using  $G_r = 30$  when  $G_r > 30$  (the equations are not formulated for use with greater values of  $G_r$ ). The parameter  $C_G$  is equal to 1.0 for circular discrete columns, but is less than unity for grids as discussed in the next section. The above expression reduces to the assumption of shear strain compatibility if  $\gamma_r = \gamma_c/\gamma_s$  is set equal to unity. The shear stress reduction factors computed using this relationship are compared in Fig. 6 for two cases: (a) assuming  $\gamma_r = 1$ , which is the assumption of shear strain compatibility, and (b) using the above expression for  $\gamma_r$  recommended by Rayamajhi et al. (2014). These results show that DM columns may be expected to reduce shear stresses by 10–30% for a wide range of design conditions (Fig. 6b), whereas the assumption of shear strain compatibility greatly overestimates the benefits of the column reinforcements (Fig. 6a).

Gueguin et al. (2013) developed solutions for the homogenized response of linear-elastic, periodic inclusion reinforced soil. The effect of the inclusions was expressed as a shear strain reduction factor ( $R_\gamma$ ), which is the ratio of the average shear strain in the soil for the improved case versus the unimproved case for a vertically-propagating shear wave of the same frequency and displacement amplitude. If the average equivalent shear modulus ( $G_{av}$ ) for the improved case is greater than the shear modulus for the untreated soil ( $G_s$ ), then the wave length will be longer for the treated case (since the frequency is the same) and thus the shear strains will be smaller (since the wave amplitude is the same). Upper and lower bound solutions were developed for a range of inclusion geometries. For example, the plot of  $R_\gamma$  versus  $A_r$  for  $G_r = 10$  in Fig. 7a includes three blue lines for the case of columnar inclusions; the two solid blue lines are from the upper and lower bound solutions, whereas the dashed blue line is the average of the upper and lower bound solutions. The average solution increases from  $R_\gamma = 1.0$  at  $A_r = 0$  to  $R_\gamma = 1.05$  at

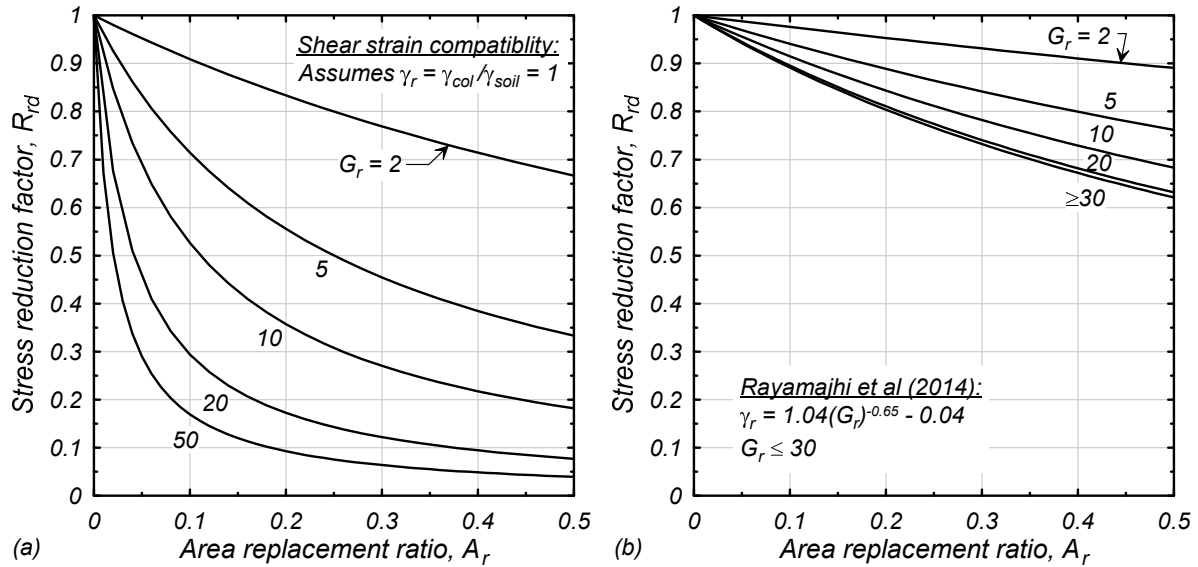


**Fig. 6. Shear stress reduction factor ( $R_{rd}$ ) for periodic arrangement of columns based on: (a) assumption of shear strain compatibility, and (b) relationship by Rayamajhi et al. (2014)**

$A_r = 40\%$  for this case, indicating that soil strains are slightly increased by the presence of the columns. The plot of  $R_\gamma$  versus  $G_r$  for  $A_r = 0.16$  in Fig. 7b, which shows only the average solution, similarly indicates that  $R_\gamma$  is a few percent greater than unity for  $G_r$  values from 1 to 45. The authors thus concluded that columnar reinforcements were relatively ineffective for reducing seismic shear stresses in soil, relative to grid reinforcements (discussed in the next section).

The solutions of Gueguin et al. (2013) are used herein to develop shear stress reduction factors for the alternative assumption that the dynamic loading produces the same average shear stress for the improved and unimproved cases. Assuming the same average shear stress is consistent with assuming the same maximum horizontal surface acceleration ( $a_{max}$ ), such that the ratio of shear stresses in the soil for improved versus unimproved cases is equivalent to the  $R_{rd}$  parameter described previously. The resulting solutions for  $R_{rd}$  can be related to Gueguin et al.'s (2013) expressions for  $R_\gamma$  as,

$$R_{rd} = R_\gamma \left( \frac{G_s}{G_{av}} \right)^{0.5} \quad [5]$$

The plot in Fig. 8a shows the upper bound, lower bound, and average  $R_{rd}$  values based on Gueguin et al.'s (2013) solutions for  $G_r = 10$  and  $A_r = 0-50\%$ . At  $A_r = 40\%$ , the average  $R_{rd}$  is about 0.75 whereas the average  $R_\gamma$  is 1.05 for this same value of  $G_r$  (Fig. 7a); the  $R_{rd}$  is smaller than  $R_\gamma$  because assuming the same average shear stress produces smaller wave amplitudes for the improved case than for the unimproved case (whereas  $R_\gamma$  is based on assuming the same wave amplitude). The average  $R_{rd}$  from Gueguin et al.'s (2013) solutions are compared to those from Rayamajhi et al.'s (2014) relationship in Fig. 8b for  $G_r$  of 2, 5, 10, 20, and 50. The  $R_{rd}$  by these two approaches are generally within a few percent of each other, which is reasonably consistent given the differences in their approaches, profiles, properties, and loading conditions.

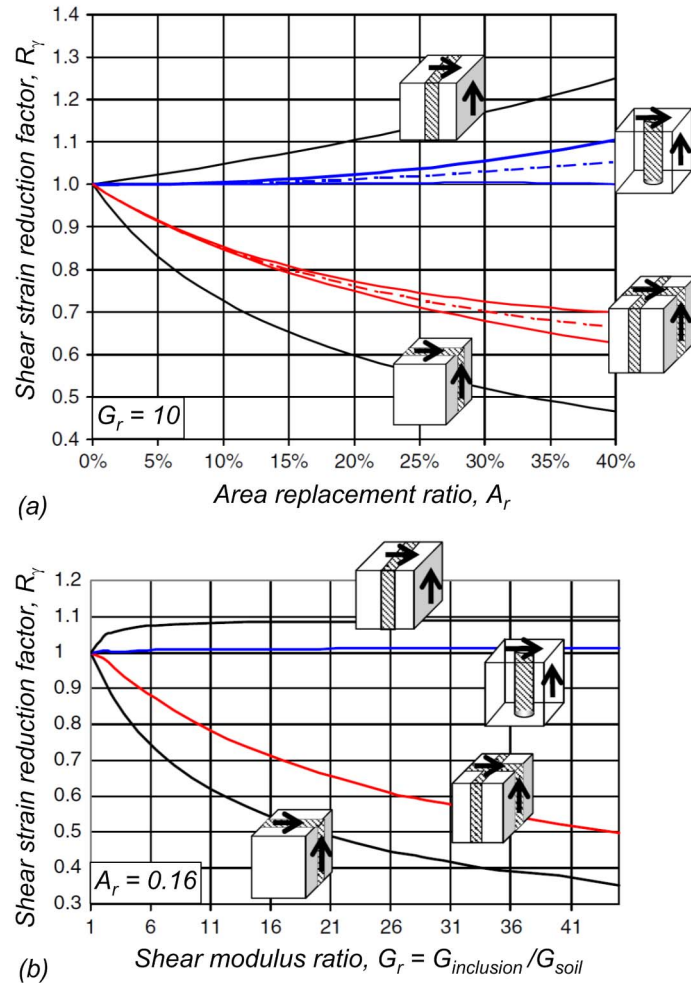


**Fig. 7. Shear strain reduction factor ( $R_\gamma$ ) from homogenization theory for linear elastic behavior of periodic inclusion-reinforced soil with the same amplitude, vertically propagating, horizontal shear wave for unimproved and improved cases: (a) variation in  $R_\gamma$  for different area replacement ratios  $A_r$  at a shear modulus ratio  $G_r = 10$ , (b) variation in  $R_\gamma$  for different  $G_r$  with  $A_r = 0.16$  (Gueguin et al. 2013, modified for notation)**

Nonlinearity or yielding in the DM columns would reduce their effective stiffness, but the above findings are not likely to be affected. For example, Rayamajhi et al. (2016) performed 3D NDAs for dense granular columns, and found that accounting for nonlinearity in the native soil and granular columns did not affect the general conclusions. Their results for a range of  $G_r$ ,  $A_r$ ,  $L/D$  ratios, ground surface pressures, relative densities, and ground motions were consistent with the design relationship originally derived from linear elastic solutions. These analysis results suggest that including nonlinearity in DM columns would lead to solutions consistent with those from linear elastic solutions.

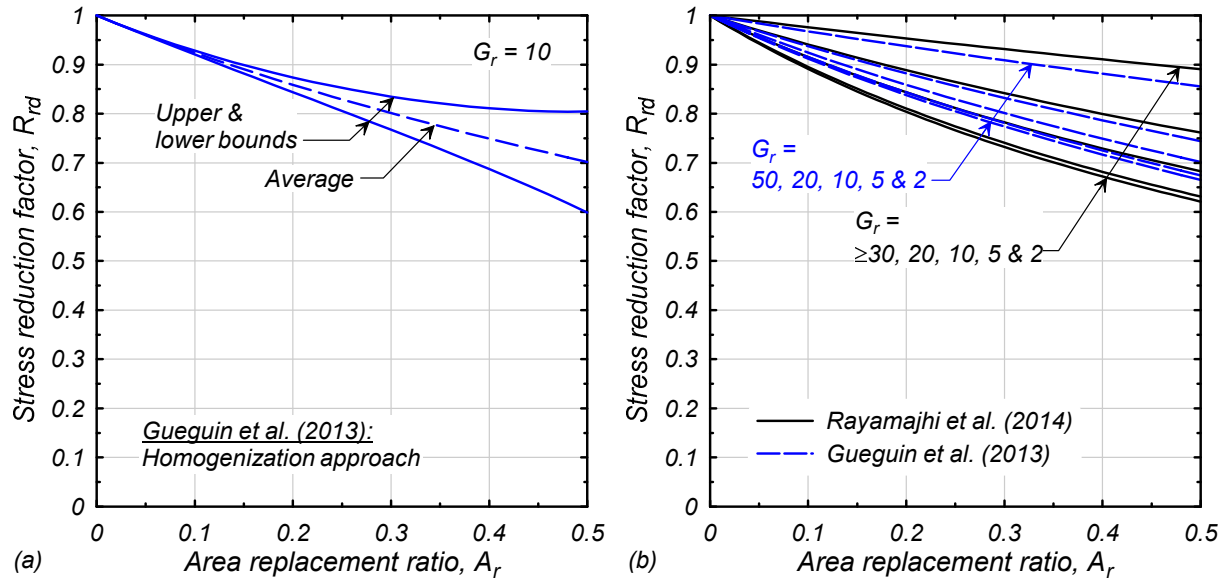
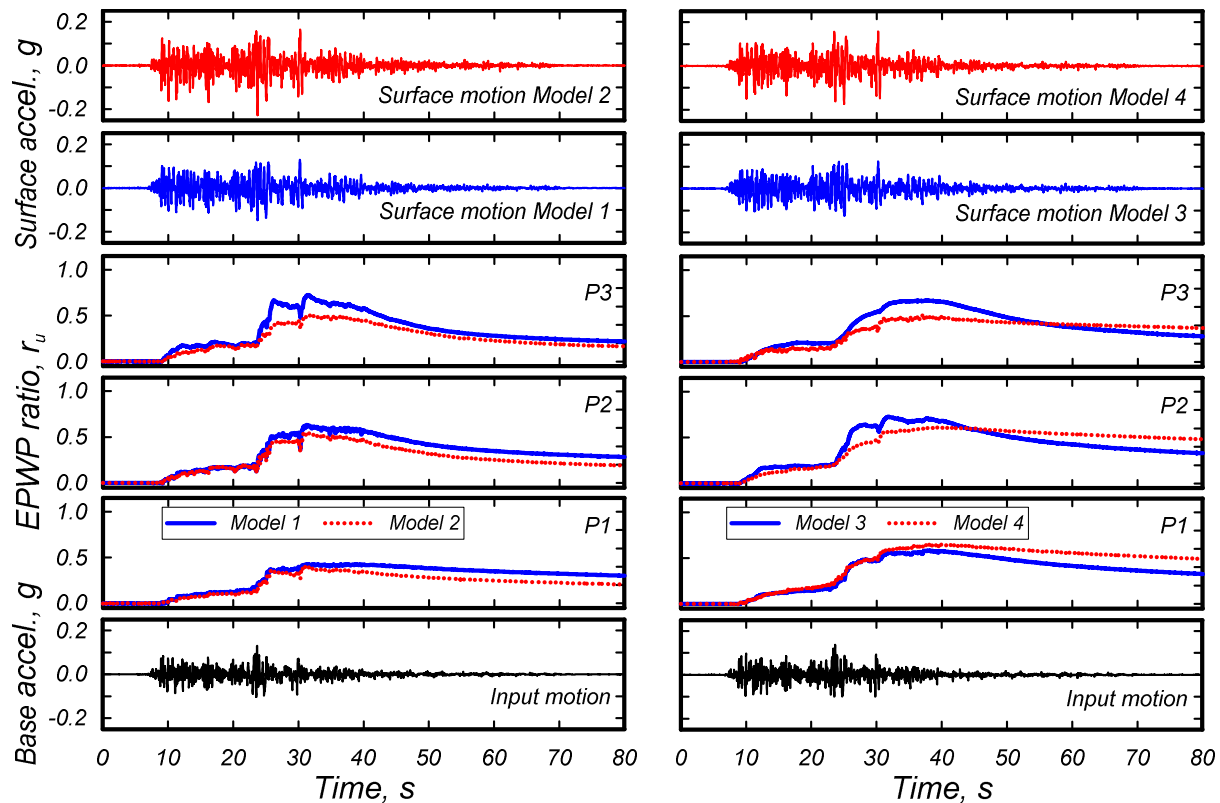


**Fig. 8. Shear stress reduction factor ( $R_{rd}$ ): (a) upper bound, lower bound, and average  $R_{rd}$  values for  $G_r = 10$  using Gueguin et al.'s (2013) solutions, and (b) average  $R_{rd}$  using Gueguin et al.'s (2013) solutions and Rayamajhi et al.'s (2014) relationship**

Four centrifuge tests were performed by Rayamajhi et al. (2015a, 2015b) to investigate the reinforcing mechanisms of soil-cement columns in level profiles of liquefiable sand. Two unimproved baseline models (models 1 and 3) and two models improved with soil-cement columns (models 2 and 4) were subjected to sine sweep and earthquake base motions. The soil profiles had 8 m (prototype dimension) of loose sand overlying either dense sand (models 1 and 2) or cemented sand (models 3 and 4). Soil-cement columns with 1.75-m diameters were spaced to give  $A_r = 30\%$  and rested on top of the dense sand in model 3 (free base condition) versus being embedded in the cemented sand in model 4 (fixed base condition). Acceleration and pore pressure measurements during various shaking events, as illustrated by those for shaking event 8 in Fig. 9, showed that the column reinforcements did not significantly reduce the excess pore pressures for the same input motions. For stronger shaking events (shown in Rayamajhi et al. 2015a), liquefaction triggering occurred at nearly the same time for both unimproved and improved soil cases and the magnitude of the resulting soil settlement was not significantly reduced. These model tests showed that the discrete columns were not effective at preventing liquefaction triggering or soil settlements, but they did show that the columns remained intact and did not settle significantly themselves, such that the columns could have provided support for overlying structures even after liquefaction triggering.

Demir and Ozener (2019, 2020) performed 2D and 3D NDAs of the centrifuge model tests by Rayamajhi et al. (2015a). The analyses by Demir and Ozener (2019) were performed using Plaxis (2016) with the nonlinear UBC3D-PLM model for the liquefiable soils and linear elasticity for the soil-cement columns, whereas the analyses by Demir and Ozener (2020) were performed using OpenSees with the nonlinear PDMY02 and PIMY models (Yang et al. 2003) for the liquefiable soil and soil-cement columns, respectively. The numerical analysis results from both studies were in reasonable agreement with the centrifuge test results, and indicated that the shear strains in the columns were far smaller than in the native soil ( $\gamma_r \approx 0.02-0.03$ ) and that the columns did not significantly reduce the dynamic shear stresses or slow the generation of excess pore pressures in the native soil.



(a) Model 1 versus Model 2

(b) Model 3 versus Model 4

**Fig. 9. Acceleration and excess pore pressure time histories for the same shaking motion for centrifuge models of level, saturated sand with 8 m (prototype) of loose sand overlying either dense sand (models 1 and 2) or cemented sand (models 3 and 4), with or without 1.75-m diameter soil-cement columns spaced to give  $A_r = 30\%$ : (a) untreated soil (model 1) versus soil treated with columns resting on the top of the dense sand layer (model 2), and (b) untreated soil (model 3) versus soil treated with columns embedded in the cemented sand (model 4) (Rayamajhi et al. 2015b)**

Rayamajhi et al. (2015a, 2015b) used acceleration records from the above centrifuge tests to define the effective natural frequency of the profiles and to obtain the dynamic stress-strain responses for unimproved and improved soil. When the bases of the columns were free to rotate, the columns rocked within the soil and produced negligible shear stiffening of the soil profile. When the bases of the columns were fixed against rocking and the columns had not yet cracked, the columns deformed in both shear and flexure, which increased the stiffness of the soil profile. The design equations by Rayamahji et al. (2014) and Gueguin et al. (2013) provided reasonable estimates for the observed natural frequency of the model with fixed-base columns, but overestimated the observed natural frequency of the model with free-base columns. While the equations by Rayamajhi et al. (2014) produced results in better agreement with the fixed-based columns than the free-base columns, the equations were in fact derived for conditions wherein the column bases, although founded on stiffer soils, were free to rotate. The assumption of shear strain compatibility greatly over-estimated the average shear stiffness for the treated soil.

The average shear stiffness of a treated soil profile can also be used to estimate the average shear wave velocity for vertical propagating shear waves. Using Rayamajhi et al.'s (2014) expressions, the average shear stiffness of a treated soil profile can be approximately estimated as,

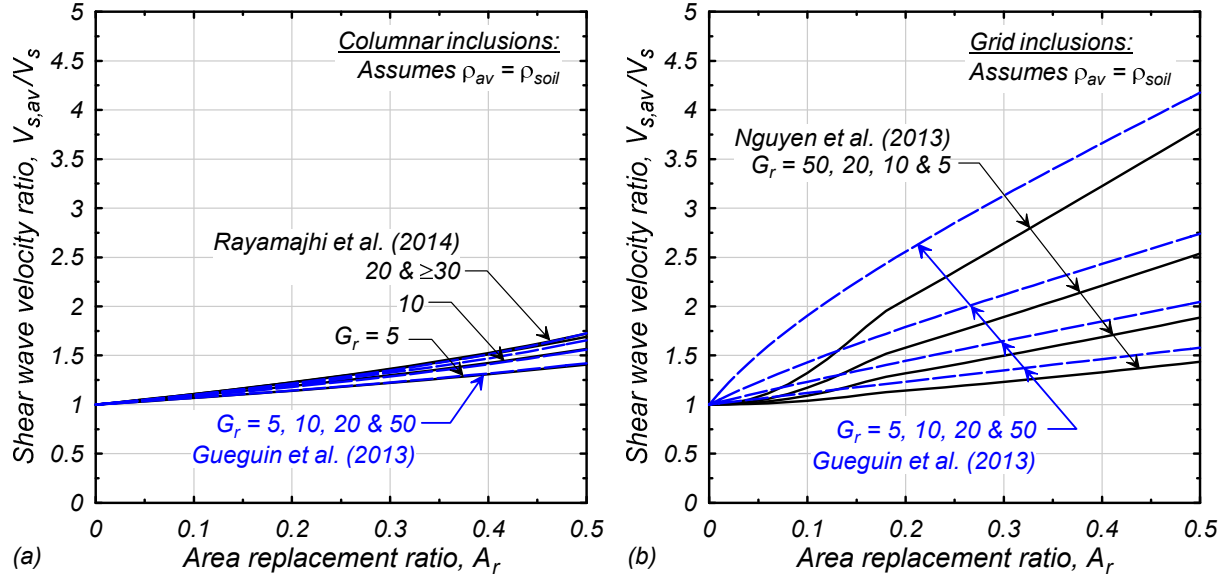


**Fig. 10. Shear wave velocity ratio for soil with periodic inclusions: (a) columnar inclusions based on relationships by Gueguin et al. (2013) and Rayamajhi et al. (2014), and (b) grid inclusions based on relationships by Gueguin et al. (2013) and Nguyen et al. (2013)**

$$G_{av} = \frac{\tau_{av}}{\gamma_{av}} = \frac{G_s \gamma_s (1 - A_r) + G_c \gamma_c C_G A_r}{\gamma_s (1 - A_r) + \gamma_c A_r} = \frac{G_s \gamma_s [(1 - A_r) + G_r \gamma_r C_G A_r]}{\gamma_s [(1 - A_r) + \gamma_r A_r]} \quad [6]$$

$$\frac{G_{av}}{G_s} = \frac{1 + A_r (G_r \gamma_r C_G - 1)}{1 + A_r (\gamma_r - 1)} \quad [7]$$

The average shear wave velocity for vertically propagating shear waves in the treated soil ( $V_{s,av}$ ) can then be estimated as,

$$V_{s,av} = \sqrt{\frac{G_{av}}{\rho_{av}}} = \sqrt{\left( \frac{1 + A_r (G_r \gamma_r C_G - 1)}{1 + A_r (\gamma_r - 1)} \right) \frac{G_s}{\rho_{av}}} \quad [8]$$

The ratio of  $V_{s,av}$  to the soil's shear wave velocity ( $V_s$ ) is therefore,

$$\frac{V_{s,av}}{V_s} = \sqrt{\left( \frac{1 + A_r (G_r \gamma_r C_G - 1)}{1 + A_r (\gamma_r - 1)} \right) \sqrt{\frac{\rho_s}{\rho_{av}}}} \quad [9]$$

Estimates for the average shear stiffness of the treated soil can also be obtained by averaging the upper and lower bound solutions by Gueguin et al. (2013), which in turn can be used to estimate  $V_{s,av}$ . The  $V_{s,av}/V_s$  ratios obtained using the expressions by Rayamajhi et al. (2014) and Gueguin et al. (2013) for sites treated with columnar inclusions are compared in Fig. 10a for a range of  $A_r$  with  $G_r$  values of 5, 10, 20, and 50. Results obtained using these two approaches are in good agreement, and together indicate that  $V_{s,av}$  might be only 20–50% greater than  $V_s$  for a broad range of columnar treatment configurations.

Rahmani and Baez (2020) recently developed an expression for  $V_{s,av}/V_s$  that approximated results of 2D and 3D linear-elastic finite element analyses for columnar treatments. Their expression was based on an equivalent average travel time for shear waves propagating horizontally across the column treated area,

$$\frac{V_{s,av}}{V_s} = \frac{1}{1 - A_r \left( 1 - \frac{1}{n_v} \right)} \quad [10]$$

where  $n_v = V_{s,c}/V_s$ , and  $V_{s,c}$  = shear wave velocity of the column material. If the densities of the column material and soil are equal, then  $n_v$  is equal to the square root of  $G_r$ . For the range of conditions presented in Fig. 10a, the  $V_{s,av}/V_s$  values obtained using this expression were within -4% to -1% from those based on Rayamajhi et al. (2014). Together, these various expressions provide a rational basis for estimating the effects of columnar inclusions on seismic site response, whether by guiding selection of equivalent homogenized properties for use in one-dimensional site response analyses, or in estimating the  $V_{s30}$  (average wave velocity in the upper 30 m) required for determining a site class for use in many seismic design codes.

The average stiffness of a soil profile with DM inclusions (discrete columns or grids) was also evaluated by Ishikawa and Asaka (2006) using shaking table tests and numerical analyses. They performed 1 g shaking table tests of a level profile of dry sand treated with columns or grids, and developed solutions for the equivalent shear stiffness of the treated profiles using a homogenization method and eigenvalue analysis. The results of their experiments and analyses indicate that the increase in shear stiffness for a treated soil profile is far greater with grid reinforcements than with discrete column reinforcements.

Bahmanpour et al. (2019) performed 1 g shaking table tests to evaluate the effectiveness of DM columns in mitigating liquefaction for a level soil profile, and concluded they can decrease the extent of liquefaction considerably. The tests were performed in a 1-m long, 0.5-m wide, and 1-m tall laminar box. The DM columns were modeled using hollow PVC pipes with 50 mm outer diameter and 2 mm wall thickness. The PVC pipes were filled with sand to maintain mass and the bottoms were sealed to preclude them functioning as drains. The PVC pipes were fixed at the base (except for one test where the pipes only extended from the surface to mid-depth in the soil profile), and were either fixed (via connection to plate) or free against rotation at the top. Toyoura sand was placed by water sedimentation around the PVC pipes. Models were shaken with 15 seconds of sinusoidal motion comprised of 5 seconds of constant amplitude motion preceded and followed by 5-second tapers. For an area replacement ratio of 35% or 50%, the maximum pore pressure ratio was reduced to about 75–80%, compared to 100% without any columns. The authors concluded that the flexural rigidity of the columns was the most important parameter affecting their performance, and noted that the flexural rigidity of the PVC pipes was much greater than required by 1 g similitude laws. The overly large flexural rigidity of the PVC pipes combined with their fixed-base condition and resistance to flexural cracking may explain why they were more effective at reducing peak excess pore pressures than was observed with soil-cement columns in the centrifuge tests by Rayamajhi et al. (2015a,b).

The experimental and theoretical studies summarized above provide a reasonably consistent set of findings across the range of conditions examined. The equivalent shear stiffness of a soil profile with columnar inclusions can be estimated using relatively simple expressions that account for shear strain incompatibility between the columns and soil. The effect that this stiffening has on dynamic site response needs to be considered for design. The seismic shear stresses imposed on the native soil between the columns are reduced relative to those for an untreated profile with the same peak surface acceleration,

but the magnitude of the reduction is modest (e.g., less than 10–30% for typical conditions in practice). The DM columns may not be effective at preventing liquefaction triggering, but they can provide vertical support for overlying structures if their lateral movements are limited. Design methods based on the assumption of shear strain compatibility are not justified and their use should be discontinued.

### Preventing liquefaction triggering – Grids

Soil-cement grids or lattices are more effective than columns for stiffening a site and reducing strains on the enclosed soil. The effectiveness of soil-cement grids, like columns, can be expected to depend on the properties of the grid (i.e., soil-cement stiffness, wall thickness, wall height, wall spacing, and configuration), characteristics of the liquefiable strata, initial static loading conditions, and ground motion characteristics. Analysis and design approaches for grids have been proposed or discussed by numerous researchers, including O'Rourke and Goh (1997), PWRI (1999), Kitazume and Terashi (2013), Kitazume (2016), Koseki (2018), and Uchida et al. (2018). The following review examines select dependencies as identified by various researchers.

Nguyen et al. (2013) performed linear-elastic 3D dynamic analyses to develop a relationship for the average shear stress reduction on the soil inside a grid. The analyses considered a unit cell for a soil profile comprised of a 1-m thick dense sand layer, over a 6–10 m thick liquefiable layer, over a 2-m thick dense sand layer (Fig. 11). The overlying and underlying dense sand layers were four times stiffer than the liquefiable layer. The grid walls were 1-m thick and extended from the bottom to the top of the liquefiable layer, such that the grid height (H) was 6, 8, or 10 m. The analyses varied the grid center-to-center spacing (S) and soil-cement stiffness to obtain a broad range of area replacement ratios ( $A_r = A_{dm}/A_t$ , where  $A_{dm}$  = area of the deep-mixed material) and shear modulus ratios ( $G_r = G_{dm}/G_s$ , where  $G_{dm}$  = shear modulus of the deep-mixed soil-cement). The subscript "dm" for the area and modulus of deep-mixed material identifies the intended application, but the solution is applicable to any wall/grid material. The analyses included pseudo-static loading and dynamic loading using harmonic input motions and earthquake ground motions. The analysis results showed that the distribution of shear stresses in the soil was affected by the H/S ratio, location within the treatment interval (horizontally and vertically), and

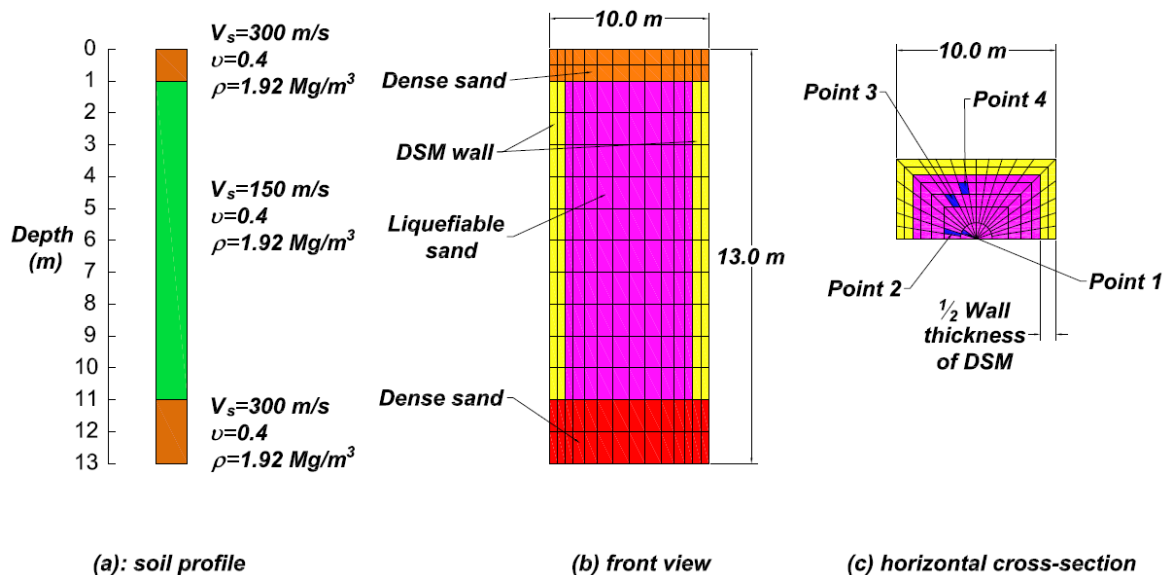
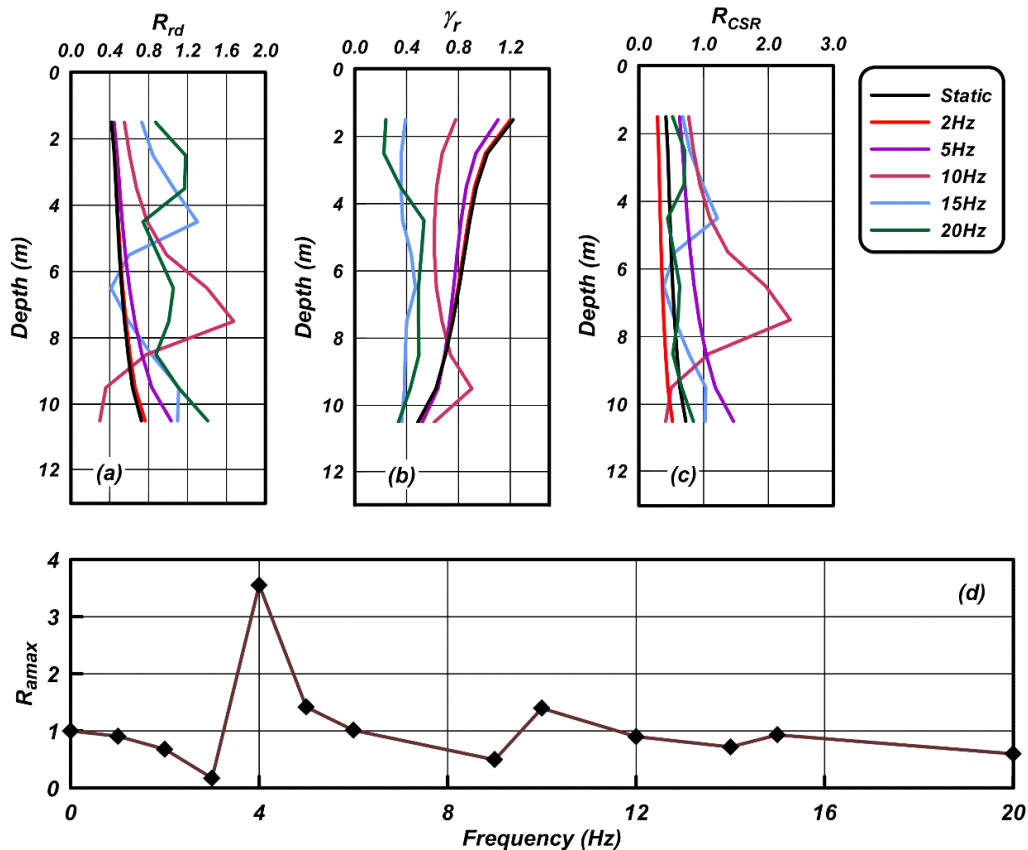


Fig. 11. Finite element model for unit cell from periodic grid arrangement with wall thickness of 1.0 m, wall spacing of 10 m, and liquefiable layer thickness of 10 m (Nguyen et al. 2013)



**Fig. 12. Effect of harmonic input motion frequency on (a)  $R_{rd}$ , (b)  $\gamma_r$ , (c)  $R_{CSR}$ , and (d)  $R_{amax}$  for wall spacing of 10 m ( $A_r = 19\%$ ) and shear modulus ratio  $G_r = 13.5$  (Nguyen et al. 2013)**

frequency content of the input motion. For example, the analysis results shown in Fig. 12 for harmonic input motions illustrate the effect of input motion frequency. Frequencies of 2 Hz or 5 Hz produce wavelengths of 75 m or 30 m, respectively, in the treated soil, which are long enough relative to the soil profile thickness that the results for  $R_{rd}$  and  $\gamma_r$  are similar to those obtained for pseudo-static loading (Fig. 12a,b). Frequencies of 15 Hz or 20 Hz produce wave lengths of 10 m or 7.5 m, respectively, in the treated soil, which are short enough relative to the soil profile thickness and wall spacing that the enclosed soil and wall motions become incoherent, which results in significantly smaller  $\gamma_r$  values and significantly larger  $R_{rd}$  values (Fig. 12a,b). The peak surface acceleration and hence  $R_{amax}$  and  $R_{CSR}$  (Fig. 12c,d) increase when the frequency is close to a fundamental frequency for the treated soil profile. Other analyses showed that larger wall spacing (corresponding to smaller  $A_r$  values) resulted in greater differences between the enclosed soil and wall motions, such that  $R_{rd}$  values increased further. The analysis results with earthquake motions, which contain a broad range of frequencies, showed trends similar to an averaging of those for harmonics in Fig. 12.

Nguyen et al. (2013) subsequently proposed the following relationships for approximating the stress reduction factors obtained from the 3D dynamic analyses across the range of conditions and earthquake motions examined,

$$R_{rd} = \frac{1}{(1 - A_r) + A_r C_G \gamma_r G_r} \leq 1 \quad [11]$$

$$C_G = 1 - 0.5\sqrt{1 - A_r} \quad [12]$$

$$\gamma_r = \left[ 1 - (1 - A_r)^{1.3} \left( \frac{G_r - 1}{185} \right)^{0.4} \right] \cdot \min \left( \frac{H}{S}, 1 \right) \quad [13]$$

where  $C_G$  = equivalent shear factor which is the shear stiffness of the grid divided by the shear stiffness it would have if it all deformed in pure shear. For example, the  $C_G$  is approximately 0.5–0.6 if the walls parallel to shaking deform primarily in shear and the walls spanning in the orthogonal direction deform primarily in flexure and contribute negligibly to system stiffness. The  $\gamma_r$  decreases (and hence  $R_{rd}$  increases) as the  $H/S$  ratio decreases below unity; i.e., the efficiency of the grid decreases when the wall spacing exceeds the height of the grid. The  $\gamma_r$  relationship does not include dependence on depth within the grid, although the analysis results did show that  $\gamma_r$  decreases (and hence  $R_{rd}$  increases) slightly with increasing depth. Instead, a single relationship for  $\gamma_r$  was developed that approximately enveloped the  $\gamma_r$  and  $R_{rd}$  at different depths within the grid. The relation between  $R_{rd}$  and  $A_r$  obtained for different  $G_r$  values using the above expression are compared to those for the assumption of shear strain compatibility (i.e.,  $\gamma_r = 1$ ) with  $C_G = 1$  in Fig. 13. The  $R_{rd}$  values from Nguyen et al. (2013) are larger than predicted by shear strain compatibility with  $C_G = 1$  because the orthogonal walls deform in flexure and the motions for the enclosed soil and walls become increasing incoherent as the wall spacing increases (or  $A_r$  decreases).

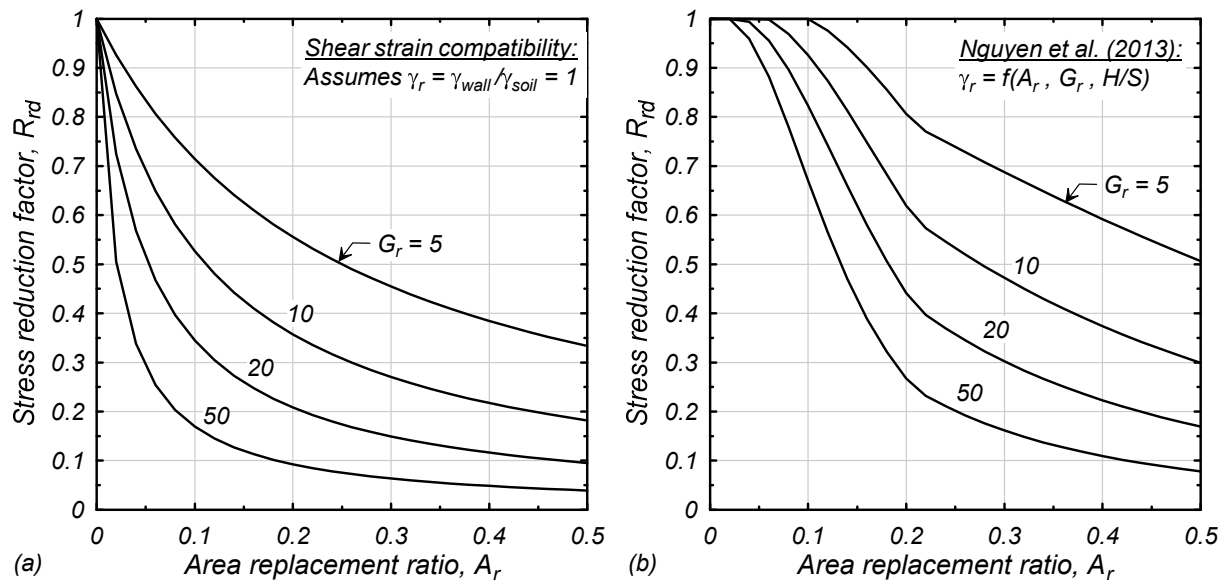


**Fig. 13. Shear stress reduction factor ( $R_{rd}$ ) for periodic grid reinforcement based on: (a) shear strain compatibility with  $C_G = 1$ , and (b) relationships by Nguyen et al. (2013)**

Gueguin et al. (2013) developed solutions for the homogenized linear-elastic response of soil reinforced with: (a) periodic walls parallel to the direction of shearing, (b) periodic walls perpendicular to the direction of shearing, and (c) periodic square grids. The shear strain reduction factor ( $R_\gamma$ ) for a given  $A_r$  was greater than unity for walls perpendicular to the loading direction, smallest for walls parallel to the loading direction, and intermediate for walls in a grid pattern (Fig. 7). These results suggest that the lateral stiffness of the grid arrangement is dominated by those walls parallel to the loading direction, and that the orthogonal walls do not contribute much to the lateral stiffness.

The solutions of Gueguin et al. (2013) are used herein to develop shear stress reduction factors for the grid system with the assumption that the dynamic loading produces the same average shear stress for the

improved and unimproved cases. The plot in Fig. 14a shows the upper bound, lower bound, and average  $R_{rd}$  values, based on Gueguin et al.'s (2013) solutions, for  $G_r = 10$  and  $A_r = 0-50\%$ . Also shown on this figure are curves for  $R_{rd}$  computed using the assumption of shear strain compatibility with  $C_G = 1.0$  (i.e., all walls deform in pure shear) and  $C_G = 0.55$  (only walls parallel to the loading direction contribute to lateral stiffness). The shear strain compatibility solution with  $C_G = 0.55$  is almost identical to the average solution by Gueguin et al. (2013).

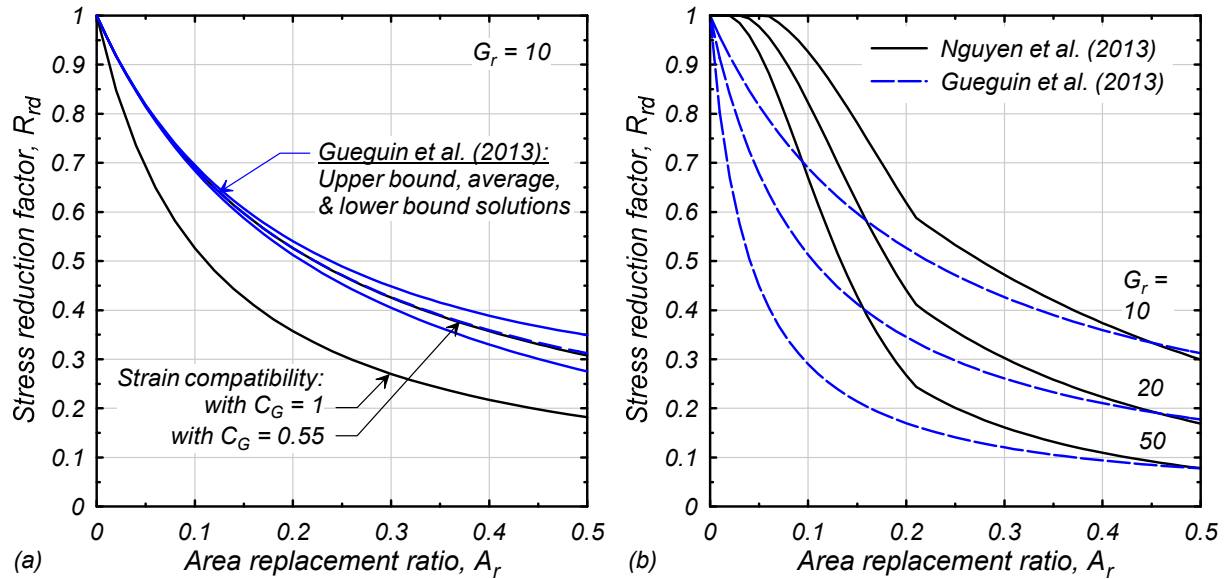


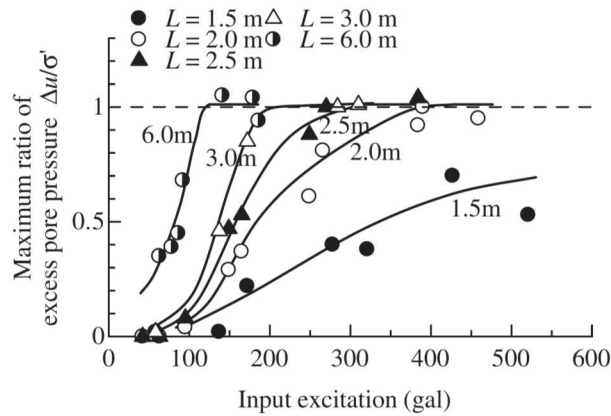
**Fig. 14. Shear stress reduction factor ( $R_{rd}$ ) for periodic grid arrangement of shear walls: (a) solutions based on shear strain compatibility with  $C_G = 0.55$  or 1.0 and the homogenization approach of Gueguin et al. (2013) for  $G_r = 10$ , and (b) solutions by Gueguin et al. (2013) and relationship by Nguyen et al. (2013) for  $G_r = 10, 20$ , and 50**

The solutions of Gueguin et al. (2013) and Nguyen et al. (2013) are compared in Fig. 14b showing  $R_{rd}$  versus  $A_r$  for  $G_r$  of 10, 20, and 50. The  $R_{rd}$  values using Nguyen et al. (2013) are significantly greater than those computed using Gueguin et al. (2013) for  $A_r$  less than about 0.2, whereas the differences become small for  $A_r > 40\%$ . The Nguyen et al. (2013) relationships give larger  $R_{rd}$  at smaller  $A_r$  because these cases correspond to relatively large wall spacings (or small  $H/S$  ratios), for which incoherent motions between the enclosed soil column and surrounding walls decrease the beneficial effects of the walls. For later comparison to other studies,  $A_r < 20\%$  corresponds to an  $H/S$  ratio less than about 1.0 (or  $S/H \geq 1$ ) in the analysis cases examined by Nguyen et al. (2013). The analysis approach of Gueguin et al. (2013) essentially assumes in-phase shearing of the soil and walls, such that it does not account for this incoherence of soil and wall motions.

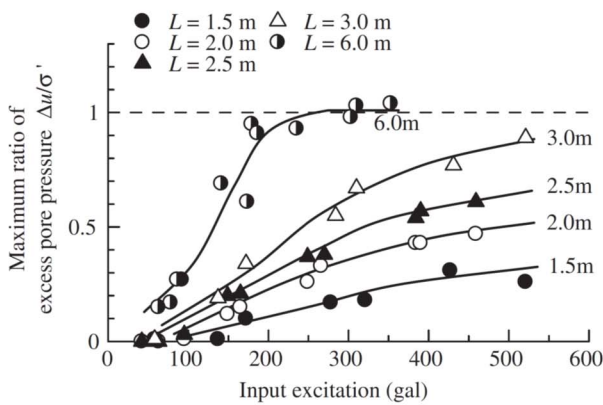
The roles of grid spacing ( $S$ ), grid height ( $H$ ), and depth with the grid ( $d$ ) have been demonstrated in a number of physical modeling studies, including several discussed in Kitazume (2016). Ishii et al. (2017) noted that one guideline derived from physical model tests (Koga et al. 1988, PWRI 1999) was that the inside spacing  $L$  (i.e.,  $L = S - t$ , where  $t =$  wall thickness) should be less than  $0.8H$  to prevent liquefaction for a peak ground acceleration of 0.21 g. The relationship between  $L/H$  and  $S/H$  depends on other dimensions, but an  $L/H$  ratio of 0.8 roughly corresponds to an  $S/H$  ratio of 0.9 to 1.0 for a range of typical geometries. Kitazume and Terashi (2013) examined data from centrifuge and shake table tests, and similarly suggested that  $S/H$  needs to be less than 0.8 for the grid to be effective at preventing liquefaction triggering. Takahashi et al. (2006) and Kitazume and Takahashi (2010) describe centrifuge model tests of submerged sand within grids constructed of bakelite panels, as shown in Fig. 15c. The centrifuge tests

were performed at a centrifugal acceleration of 25 g and used a pore fluid with a viscosity 25 times that of water. The grids had the following prototype dimensions: wall thickness of 0.5 m, wall height (or soil profile thickness) of 3.5 m, inside spacing of 1.5, 2.0, 2.5, 3.0, and 6.0 m, and depth to the pore pressure transducers of 1.0 and 2.5 m. The input motion was 50 sinusoidal cycles at 4 Hz with peak accelerations of up to 0.5 g. The maximum excess pore pressures at a depth of 1.0 m (Fig. 15a) were generally greater than at 2.5 m depth (Fig. 15b), and the maximum pore pressures at both depths decreased with decreasing  $L$ . The summary of results in Fig. 15d suggest that  $L/d$  ratios less than about 1.5–2.0 were sufficient to preclude liquefaction triggering in these tests; the corresponding  $S/H$  ratios for these tests are about 0.6–0.7. Takahashi et al. (2006) subsequently suggest that  $L/d$  is a better indicator of grid effectiveness for different depths in the soil profile, which suggests that grids are less effective nearer the top of the liquefiable layer than at the bottom. This latter trend is opposite to the trend in  $R_{rd}$  values obtained in the 3D dynamic analyses by Nguyen et al. (2013), wherein the stress reduction provided by the grids was actually slightly better at shallower depths (e.g., Fig. 12). This difference in trends with depth may be attributable to the experiments by Takahashi et al. (2006) being for a 3.5-m thick, submerged sand layer wherein upward diffusion of excess pore pressures can make liquefaction at shallow depths more likely (Darby et al. 2019), whereas the elastic analyses by Nguyen et al. (2013) included a 1-m thick stiffer crust layer over a 6-m to 10-m thick layer of sand and did not account for excess pore water pressure diffusion. Suzuki et al. (1991) performed centrifuge tests of saturated sands within grids of different  $L/H$  ratios, and showed that the potential for liquefaction at different depths within the grids was significantly reduced by lowering the water table to a modest depth below the ground surface (i.e., to a depth of  $H/10$ ). Despite the above differences in how results may vary with depth in the grid, the above experimental results are qualitatively consistent with the design relationship by Nguyen et al. (2013), which includes a term that rapidly reduces the benefits of the grid as  $S/H$  increases above 1.0 (Eq. 10). This  $S/H$  term is the primary reason why the stress reduction factors by Nguyen et al. (2013) are much greater than those computed using Gueguin et al.'s (2013) solution at  $A_r$  less than about 0.2 (Fig. 14b).

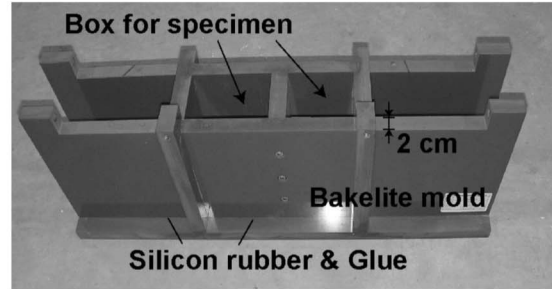
The average shear stiffness and shear wave velocity for vertical propagating shear waves in a soil treated with periodic grid inclusions can also be estimated using the approaches by Nguyen et al. (2013) and Gueguin et al. (2013). Nguyen et al.'s (2013) expressions for  $C_G$  and  $\gamma_r$  (Equations 12 and 13) can be used with Equation 7 to estimate the average shear stiffness and Equation 9 to estimate the average shear wave velocity; note that the simpler Equation 10 was derived for columnar inclusions and is not applicable for grid inclusions. Gueguin et al.'s (2013) upper and lower bound solutions can be averaged to obtain an estimate for the average shear stiffness, from which  $V_{s,av}$  can be obtained. The  $V_{s,av}/V_s$  ratios obtained using the expressions by Nguyen et al. (2013) and Gueguin et al. (2013) are compared in Fig. 10b for a range of  $A_r$  with  $G_r$  values of 5, 10, 20, and 50. The  $V_{s,av}/V_s$  ratios based on Nguyen et al. (2013) are smaller than those based on Gueguin et al. (2013), which is consistent with the differences in their stress reduction factors discussed above. Despite these differences, the two approaches are consistent in indicating that grid inclusions will increase the average wave velocity far more than columnar inclusions will (Fig. 10a). These two solution methods provide a rational basis for estimating the effects of grid inclusions on seismic site response or equivalent  $V_{s30}$  values, as noted previously for columnar inclusions.



(a) At a depth of 1.0 m

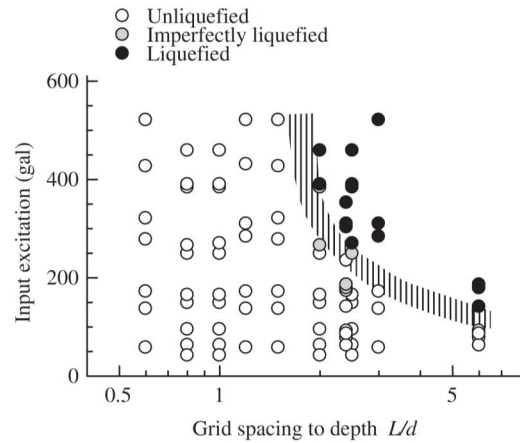


(b) At a depth of 2.5 m



d = depth from surface of saturated sand  
H = 3.5 m (full depth of sand profile)  
L = inside distance between walls

(c) Model grid and definition of dimensions



(d) Liquefaction cases for different L/d

**Fig. 15. Results of centrifuge test at 25 g with sand profile thickness of  $H = 3.5$  m (prototype), inside distance between walls of  $L = 1.5, 2.0, 2.5, 3.0,$  and  $6.0$  m, and pore pressure transducer depths of  $d = 1.0$  and  $2.5$  m (Takahashi et al. 2006)**

The stiffening of a soil profile by grid treatments has also been demonstrated by Bouckovalas et al. (2006), Papadimitriou et al. (2006), and Ishikawa et al. (2006, 2016). Bouckovalas et al. (2006) and Papadimitriou et al. (2006) compared 1D, 2D, and 3D analyses and examined approaches for producing similar seismic responses for treated soil profiles. Ishikawa et al. (2016) used an equivalent homogenization method as the basis for a simplified method for evaluating liquefaction of sandy soil confined by DM grid systems. The simplified method was shown to predict slightly lower pore pressures than those obtained in a detailed 3D finite element analysis of an example problem, with the difference attributed to the improved area being finite in the 3D model versus infinite in the homogenization method. An additional consideration would be the incoherence of motions and variations in shear strains within the treatment cells, as discussed previously.

Ishii et al. (2017) described the development of a design methodology for DM grids as a remediation measure for residential homes, for which placing a grid around the perimeter of a home generally results in  $L/H$  ratios significantly greater than unity. Centrifuge model tests were used to evaluate how the presence of the grids affected liquefaction triggering and foundation settlements. Quasi-3D and 3D finite element models were used to generalize the design methodology, which includes criteria related to the factor of safety against liquefaction triggering and foundation settlement. The design criteria use the grid area (area enclosed by a cell) rather than the grid spacing, since centrifuge tests confirmed that square or

rectangular grids with the same enclosed area produced similar responses. Other studies similarly examined the use of DM grids for protecting residential homes in areas affected by liquefaction during the 2011 Tohoku earthquake (e.g., Tsukuni et al. 2015, 2017).

Namikawa et al. (2007) performed 3D dynamic analyses of a section across a long, narrow, soil-cement grid system that was two grid boxes wide, as shown in Fig. 16a. Analyses were performed with the soil-cement modeled as elastic material (case 2a) or elastic-plastic material capable of simulating post-peak strain softening and strength loss (case 2b). The liquefiable soil was modeled using a "densification" model that combined a Mohr Coulomb yield criterion with an endochronic dilatancy model to reproduce the generation of excess pore pressure and loss of stiffness, while recognizing that the model does not simulate cyclic mobility after liquefaction has been triggered. The pattern of failed/damaged elements in the soil-cement walls after earthquake loading is shown on the oblique views in Fig. 16b. Excess pore pressures at mid-depth in the liquefiable layer within the grids are shown for both analysis cases in Fig. 16c. Excess pore pressures rose at about the same rate and reached similar maximum excess pore pressure ratios of about 0.65 in these two analysis cases, whereas liquefaction was expected to occur relatively early in shaking outside the grids (i.e., in the free field). These results suggest that localized damage to the soil-cement walls did not significantly affect their ability to limit pore pressure generation in the enclosed soils (Namikawa et al. 2007).

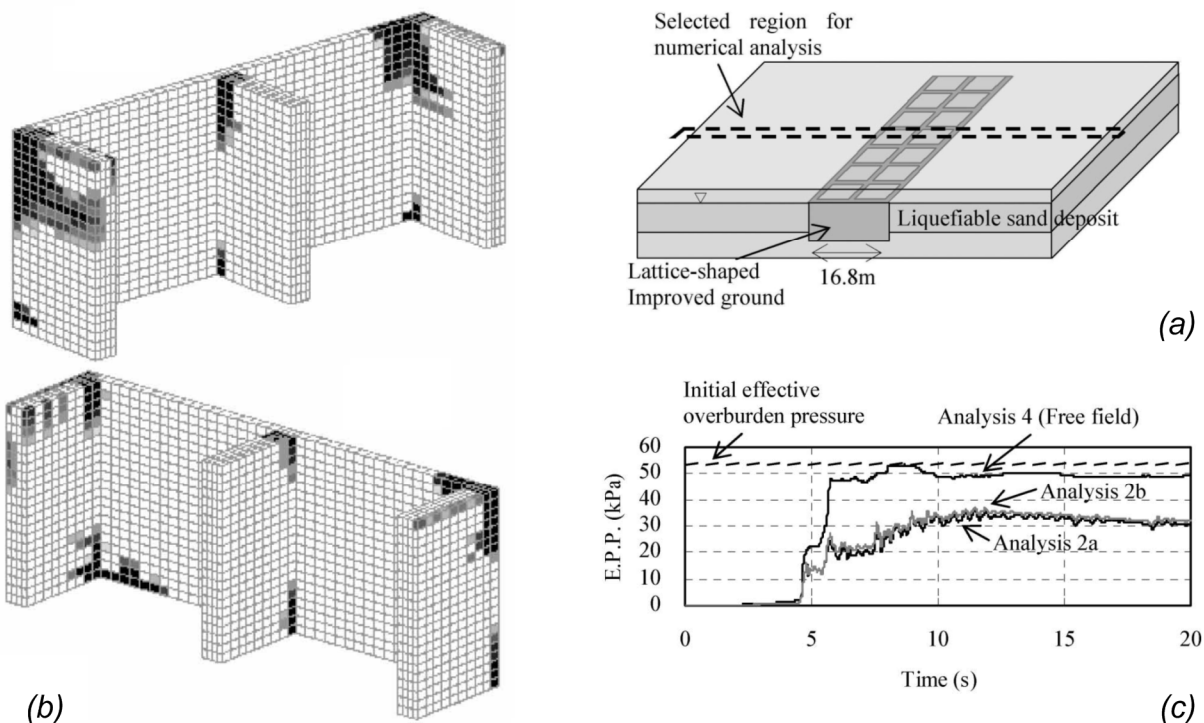


**Fig. 16. Three-dimensional finite element modeling of a soil-cement grid system by Namikawa et al. (2007): (a) geometry of treatment grid and selected region of analysis, (b) failure zones in the grid walls for analysis case 2b using an elastic-plastic material model for the soil-cement, and (c) excess pore pressures at mid-depth in the liquefiable soil in the free-field and inside the grids for analysis case 2a with elastic walls and analysis case 2b with elastic-plastic walls**

Bradley et al. (2013) performed 3D dynamic analyses of soil-cement grids in a level site that was modeled after the soil profile at the downhole array on Port Island in the 1995 Kobe earthquake. The treatment area was 24 m by 24 m in plan-view, with the grid system being a single cell, 4 cells (2 by 2 grid), or 9

cells (3 by 3 grid) as shown in Fig. 17a. Three different wall thicknesses were used for each grid configuration. The finite element model used symmetry about the x-axis with shaking only in the x-direction to reduce the mesh in half (Fig. 17b). The liquefiable soil was represented by the nonlinear, coupled, stress-density S-D model of Cubrinovski and Ishihara (1998). The soil-cement was modeled as linear elastic. The authors concluded that peak horizontal displacements, shear strains, pore pressures, and vertical settlements of the soil within the grid cells were better correlated to the improvement length-to-height ratio rather than to the improvement area ratio. The "length" referred to the clear span between adjacent walls, and the "height" referred to the full 18 m height of the walls (Fig. 17). The authors showed that the peak horizontal displacement of the soil-cement walls was greater for the walls transverse to the shaking direction (Fig. 18a,b) than for the walls parallel to the shaking direction (Fig. 18c,d), and that these wall displacements were generally better correlated to the improvement area ratio than to the improvement length-to-height ratio. Soil improvement increased the surface motions at moderate to long periods, with smaller increases at short periods; thus, the improvement would also result in greater inertial loads for an overlying structure relative to the unimproved case.

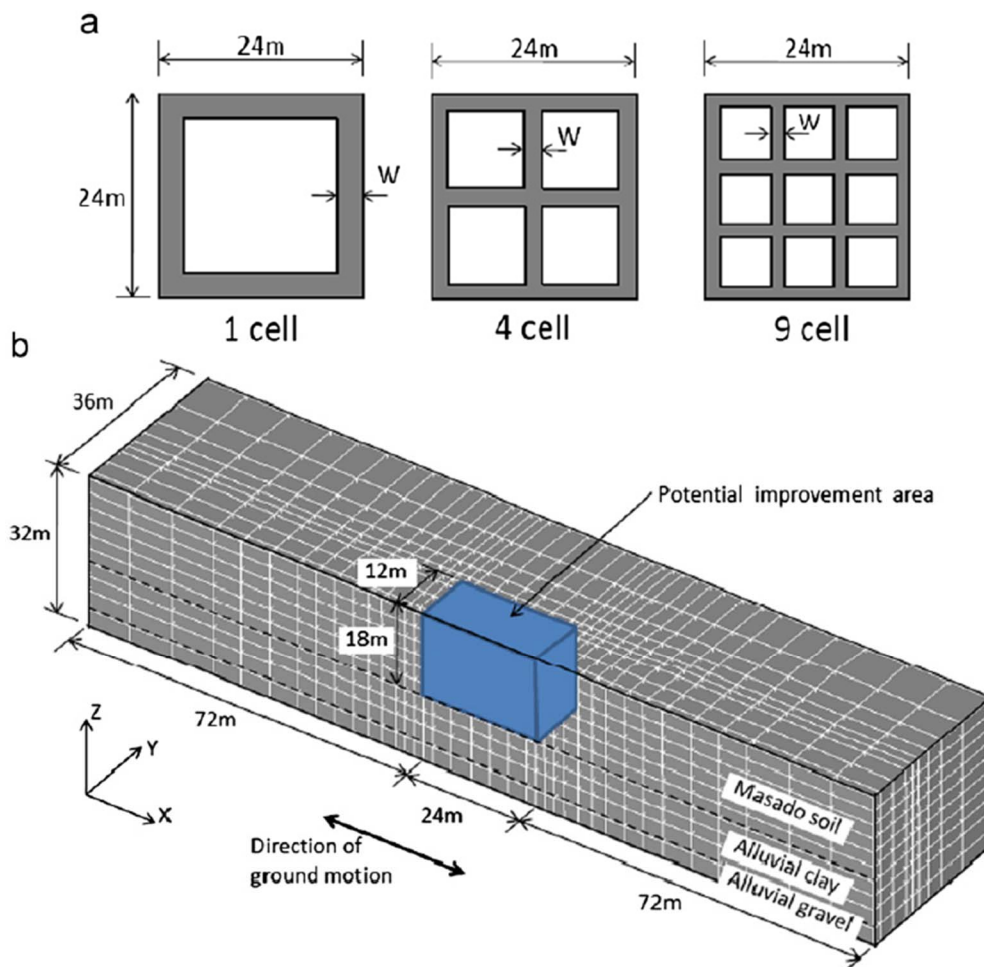


**Fig. 17. Finite element model of soil-cement grid by Bradley et al. (2013): (a) plan views of 1, 4, and 9 cell systems, (b) schematic of model allowing for symmetry about the x axis**

A basic assumption for the above studies of the seismic performance of soil-cement grids or lattices is that the walls or panels have sufficient continuity in both the horizontal and vertical directions to transfer static and seismic shear forces. Vertical joints in soil-cement walls constructed as overlapping columns have a smaller area ratio (along the chord of their overlap) compared to the average area ratio for

horizontal planes. Yielding of the walls under lateral loading may initiate along these vertical joints due to their lower area ratio and possibly lower shear strength at any cold joints. The design procedures in Bruce et al. (2013) for embankments on overlapping DM columns under static loading conditions includes different recommended factors of safety for failure modes involving shearing on horizontal planes versus vertical planes in the DM zone, with shearing along vertical planes being evaluated based on the overlapping chord area. Seismic designs often allow for yielding in the DM treatments, which may involve yielding along both horizontal and vertical planes at larger deformations. In this case, the system's lateral strength may depend on both the horizontal replacement area and vertical overlapping chord area when using overlapping columns. Soil-cement walls constructed using trench cutting and remixing deep (TRD) or cutter soil mixing methods have the advantage that they are expected to produce similar strengths along horizontal and vertical planes.

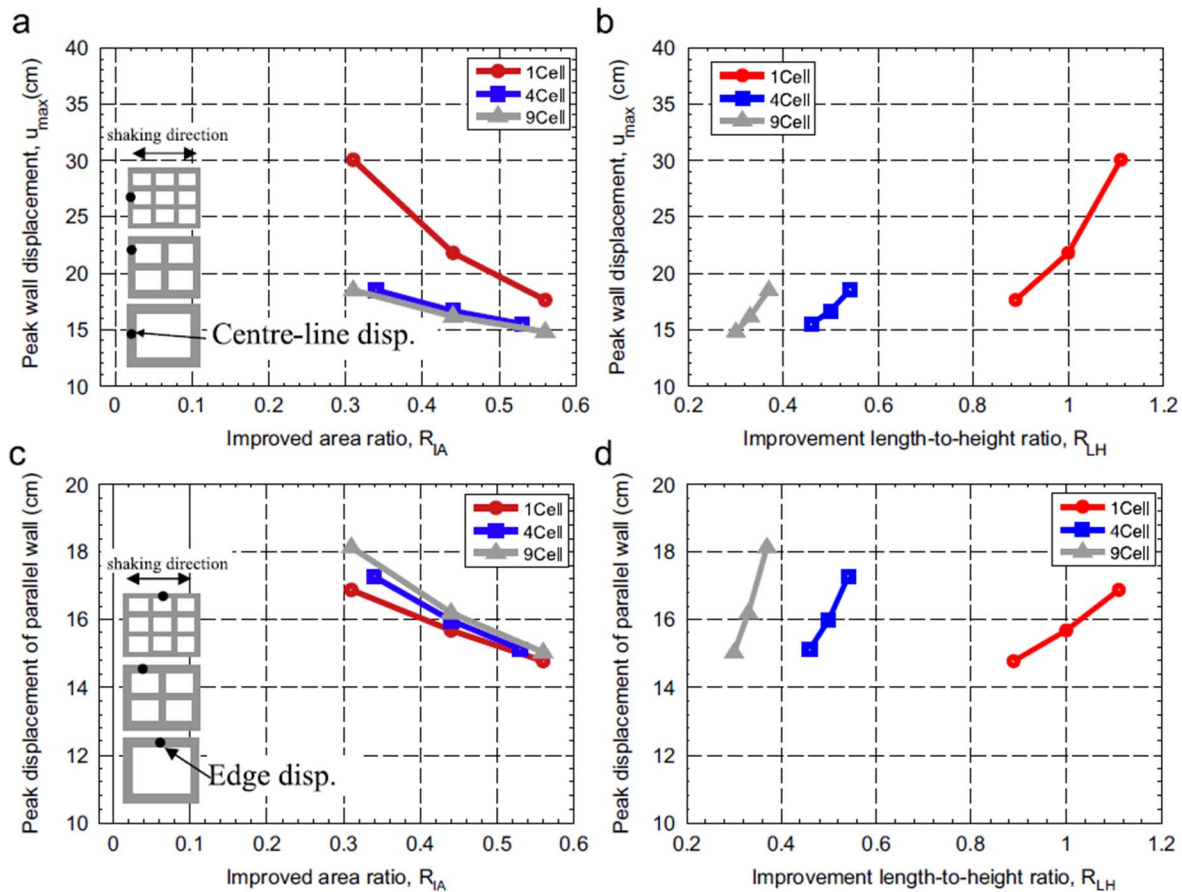


**Fig. 18. Peak horizontal displacements at the top of the soil-cement grids: (a) displacements for midpoints on the transverse walls versus improved area ratio, (b) displacements for midpoints on transverse walls versus improvement length-to-height ratio, (c) displacements for midpoints on the longitudinal walls versus improved area ratio, (d) displacements for midpoints on longitudinal walls versus improvement length-to-height ratio (Bradley et al. 2013)**

The experimental and theoretical studies summarized above demonstrate the effectiveness of DM grids for liquefaction mitigation across a broad range of conditions. The equivalent shear stiffness of a soil profile with grid treatments can be estimated using relatively simple expressions that account for shear strain incompatibility between the soil-cement and soil. The effect that this stiffening has on dynamic site response needs to be considered for design. The seismic shear stresses imposed on soil inside the grids can be significantly reduced from those for an untreated profile with the same peak surface acceleration.

This reduction in seismic shear stresses on the enclosed soil diminishes with increasing grid spacing if the spacing exceeds the height of the grids. DM grids can also help reduce foundation settlements, should liquefaction be triggered within the enclosed soils.

The results of a liquefaction triggering evaluation for a DM grid treatment using the above summarized procedures must be checked for consistency with the shear deformations estimated from any system-level response analysis. Shear deformations from a system-level response analysis, such as obtained from a 2D or 3D dynamic analysis, can be significantly different from that obtained using a unit cell analysis depending on the system and treatment geometries. For example, DM grids are sometimes placed in limited areas for reducing lateral spreading or embankment deformations (as discussed in following sections). In these cases, the DM grids are sometimes predicted to develop significant shear deformations due to their interactions with the surrounding soils or structures. Significant deformation in the DM grid will be accompanied by similar levels of shear deformation in the enclosed soils. If the strain levels from a system-level analysis are significantly greater than predicted by the above-described liquefaction triggering evaluations, then the results of the liquefaction triggering evaluation will be unconservative and are generally not applicable.

### ***Reducing lateral spreading and embankment displacements***

DM improvements may also be designed to reduce lateral spreading of mildly sloping ground (e.g., Fig. 2a,d) or reduce deformations in embankments or slopes (e.g., Fig. 2b) in the event that liquefaction is triggered in the enclosed or adjoining soils. DM treatments may be configured as a buttress zone that reduces the potential for lateral spreading in the untreated area adjacent to it (e.g., Fig. 2d), or the DM may be configured around/beneath a structure to protect its foundation against lateral spreading (e.g., Fig. 2c,e,f). Grid or lattice configurations are better suited than discrete columns for resisting lateral ground deformations, although a combination may be appropriate in certain situations; e.g., the road embankment in Fig. 2a utilizes both discrete columns and a grid, with the grid portion on the open-channel side toward which lateral spreading would develop. The demands imposed on the DM improvements, and hence their design, depend on the specific application, soil properties, seismic loading, and performance objectives.

The effect of discrete column reinforcements on reducing lateral deformations in sloping liquefiable ground were evaluated in a series of centrifuge model tests by Morikawa et al. (2015) and Takahashi et al. (2015, 2016). The centrifuge tests by Morikawa et al. (2015) used twelve acrylic piles with outer diameters of 2 m (prototype) arranged to produce an  $A_r$  of 35% in an 11.5–15 m thick soil profile. The pile tips were pinned, while the pile heads were free, pinned, or fixed. The centrifuge tests by Takahashi et al. (2016) used aluminum piles with outer diameters of 0.75 m (prototype) arranged to produce an  $A_r$  of 9–20% in a 9.1–17.3 m thick liquefiable layer. The pile tips were fixed. In both sets of centrifuge tests, the effect of irregular versus regular pile arrangements on lateral deformations was examined. The centrifuge test results and supporting numerical analyses indicate that the piles were effective at reducing but not preventing lateral displacements (relative to the unimproved cases) and that irregular pile arrangements were slightly more effective than regular arrangements (e.g., about 10% smaller lateral displacement for irregular arrangements in the tests by Takahashi et al. 2016). These findings are for piles that remained elastic during lateral loading. These results suggest that DM columns may provide some reduction in lateral spreading displacements, but the benefits would likely be much smaller (unless the columns are reinforced) because unreinforced DM columns are more likely to crack in flexure and are more difficult to restrain against rotation at their bases.

Khosravi et al. (2020) performed a centrifuge test at 50 g of an 8.5-m (prototype) tall embankment of dense sand over a 5.0-m thick liquefiable sand layer reinforced with discrete soil-cement columns beneath the lower half of the embankment slope. The soil-cement had an average  $q_u$  of 3.7 MPa, the columns were fixed in a concrete base, and the  $A_r$  was 27% for the treatment zone. The model was shaken with a scaled earthquake motion having peak base accelerations of 0.03 g, 0.4 g, and 0.55 g. The second event triggered liquefaction in the liquefiable sand layer in the toe area and between the soil-cement columns, caused cracking in the soil-cement columns, and resulted in an embankment crest settlement of 0.48 m. The crack detectors and post-test dissection photographs showed that the soil-cement columns had all sheared off along their connections with the concrete base and had tilted toward the toe of the embankment.

Elgamal et al. (2009) performed 3D finite element simulations of gently sloping ground that was reinforced with either piles or stone columns. The stone columns were effective in reducing lateral spreading deformations in sand strata but were relatively ineffective for silt strata because of the differences in drainage during shaking. Piles were equally effective for either sand or silt strata. These findings are consistent with the above-described centrifuge tests by Takahashi et al. (2016). As noted above, the benefits of unreinforced DM columns would likely be much smaller because unreinforced DM columns are more likely to crack in flexure and are more difficult to restrain against rotation at their bases.

DM columns are generally far less effective than grids or panels for reducing lateral deformations of slopes because the discrete columns and column-treated zone can often deform in ways that offer less resistance to movements (Filz et al. 2012). Columns may rotate, bend, and crack, all of which reduce the shear resistance columns can provide. Column-treated zones can also collectively deform in a racking mode, which reduces the composite resistance that the treatment zone can provide. Filz and Navin (2006) and Witthoef et al. (2019) demonstrated the importance of racking in a column-treated zone through 2D nonlinear analyses of a column-supported levee over soft clay. They repeated the analyses with the levee supported on DM panels, and showed that the increase in overall slope stability was far better with DM panels than with DM columns. Their results also demonstrated that limit equilibrium analyses of column-treated zones cannot assume that the shearing resistance in the columns equals the soil-cement strength, as that assumption greatly over-estimates the lateral resistance that the treatment zone can provide (i.e., the racking mode of deformation results in a much lower shearing resistance). Zaregarizi et al. (2021) performed similar 2D nonlinear analyses of a column-supported embankment over soft clay and demonstrated that the failure modes were influenced by the spatial variability in the soil cement strengths. These findings, although developed for soft clay conditions, are equally applicable to cases with liquefiable soils.

Chai et al. (2019) describe the failure of an embankment supported by discrete DM columns in a deposit of soft clay in Saga, Japan. The authors describe the detailed soil investigations, DM design methods, embankment construction, failure event, post-failure investigation, and 3D finite element analysis. Discrete DM columns, 1.2 m in diameter at 1.93 m spacing ( $A_r$  of 31%), were installed to a depth of 13 m through the soft clay layers. The 7.38 m tall embankment was built in late 2015 with geogrid reinforcement. The Kumamoto earthquakes of April 14 and 16, 2016 produced a peak ground acceleration of about 0.1 g in the embankment region. Measurements of lateral displacements on the embankment showed an increase in the rate of movement following the earthquake. The embankment failed ten weeks later on June 23, 2016 after a 270 mm heavy rainfall. Chai et al. (2019) concluded that the DM columns failed by bending (tension) first, followed by collapse of the embankment. In addition, they noted that for embankments with a relatively low design factor of safety, relatively large deformations can develop in the embankment, which can cause cracks that reduce its shearing resistance to essentially zero. The investigation also found some DM columns defects that were not detected by the DM construction quality control program. These lessons regarding discrete column failure modes and embankment cracking,

although observed for a static failure in soft clay, are again equally applicable to cases with liquefiable soils.

For embankments dams with liquefiable foundation layers, DM grids near the embankment toes (e.g., Fig. 2b) have been used to reduce crest settlements and global deformations on several projects, including Clemson Dam (Wooten and Foreman 2005), Sunset North Basin Dam (Barron et al. 2006), Perris Dam (Friesen and Balakrishnan 2012), San Pablo Dam (Kirby et al. 2010), and Chabot Dam (EBMUD 2020). For these and other projects, the DM treatments were designed using 2D models with composite properties in the out-of-plane dimension for the treatment zone. Boulanger et al. (2018) presented data from a centrifuge model of an embankment on a liquefiable layer treated with soil-cement walls, and showed that a 2D NDA using composite properties for the treatment zone gave reasonable agreement with the observed responses. This model test and the analysis methods are discussed in a later section.

For a transit line in an area of gently sloping ground with both liquefiable and soft soils, Azizian et al. (2017) used shear panels (comprised of overlapping DM columns), spaced nominally 5 m on centers and extending to depths of 10–24 m below ground surface, to support a transit line. They performed 2D NDAs with a ubiquitous joint model for the DM treatment zone to simulate potential planes of weakness due to progressive cracking. The soils were modeled using the constitutive models UBCSAND and UBCHYST. This approach to modeling the effects of cracking and strain softening in the DM treatment zone introduces mesh dependency and has other numerical limitations, but the approximate inclusion of this effect provides valuable insights and improvements over models that ignore these effects.

### ***Supporting or protecting overlying structures***

DM improvements may also be designed to support overlying structures or protect foundations against the effects of liquefaction and lateral spreading or ground lurch (e.g., Fig. 2c,f). Grid or lattice configurations are generally better suited than columns for either supporting or protecting overlying structures, but there are situations where either, or a combination of both, may be appropriate.

The use of DM columns for vertical load carrying capacity despite liquefaction of the native soils requires careful consideration of the significant uncertainties in estimating transient lurching or permanent lateral ground displacements. Transient lurching due to liquefaction can be estimated using the simplified procedures by Tokimatsu and Asaka (1998). Permanent lateral displacements have been observed to extend to much larger distances from a free face than some empirical relationships predict; the actual variation of displacement with distance from a free face depends on the geologic conditions, which are not adequately accounted for in some relationships (Cubrinovski and Robinson 2016). With an appropriately conservative estimate for potential lateral displacements, the DM columns must be checked for the additional bending moments induced in the columns (i.e., the P-delta effect). For these reasons, the potential utility of DM columns for vertical load carrying is best limited to situations involving larger diameter columns, column clusters, and areas of relatively small lateral displacements (i.e., avoiding large P-delta effects). If there is any concern that lateral movements could be larger than estimated, the configuration is best altered to include panels or grids because the additional costs are generally small relative to the potential benefits.

Takahashi et al. (2013) performed centrifuge model tests and numerical analyses of "fixed" and "floating" DM grids in a level deposit of liquefiable soil. Fixed grids extended down through the liquefiable layer to a stronger non-liquefiable layer. Floating grids only penetrated the upper portion of the liquefiable layer, and thus did not extend to a stronger layer. The centrifuge test results showed that the floating grids reduced the surface settlement by amounts that increased with increasing grid-penetration depth. These

tests did not include an overlying structure, but it seems reasonable to expect that floating grids could provide vertical load carrying capacity for shallow foundations in addition to reducing liquefaction-induced settlements.

Yamashita et al. (2016) described a case history of a seven-story building supported on a friction-piled raft foundation in combination with DM grids ( $A_r$  of 10%) at a site with loose sandy soil (liquefiable between depths of 6 and 11 m), underlain by soft clayey soil to a depth of 42 m, shaken during the 2011 Tohoku earthquake. The PGA was 0.12 g at the first floor. The overall performance of the facility was good, with the foundation settlement of 6 mm attributed to moment loading from the structure onto the piles. There was no evidence of liquefaction in the areas adjacent to the building, although there were some traces of liquefaction 150–200 m away from the building.

Yamashita et al. (2018) performed 3D finite element analyses of a piled-raft foundation combined with DM grids supporting a 12-story base-isolated building (Fig. 19). The DM grids were intended to prevent liquefaction of a silty sand between depths of 3 and 7 m as well as provide support for the raft. The DM grids, with an  $A_r$  of 25%, were modeled using a nonlinear elastic model with tensile and shear criteria. The analysis model was validated against the recorded responses of the building and its piles during the 2011 Tohoku earthquake, for which the peak ground acceleration at the site was about 0.18 g. The analysis model was then used to evaluate performance of the structure under a higher design level loading. For those analyses, the DM grids reduced demands on the piles because they altered the site response and helped carry lateral loads, even though the grids developed tensile and shear failure zones during strong shaking.

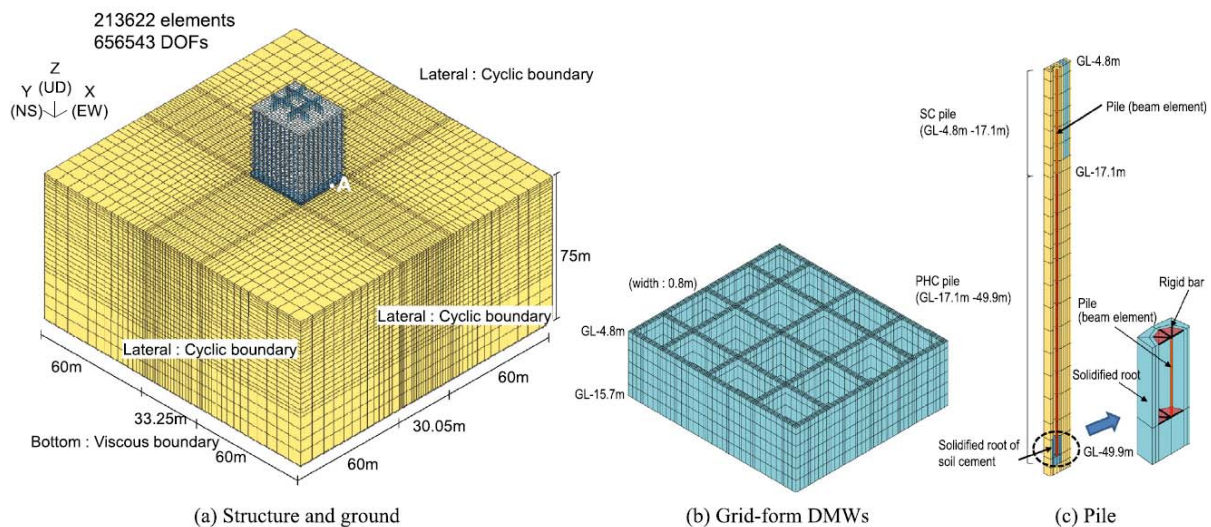


**Fig. 19. Three-dimensional finite element model for 12-story base-isolated building on a piled-raft foundation combined with a grid of DM walls (Yamashita et al. 2018)**

Other experimental and numerical studies have similarly demonstrated the effectiveness of DM treatments for supporting overlying structures or protecting them from lateral ground deformations. Kitazume et al. (2000) performed centrifuge model tests of columns subjected to different combinations of vertical and horizontal loads, from which different types of failure modes were identified. Khosravi et al. (2017, 2019) performed dynamic centrifuge model tests of structures on shallow foundations that were supported by DM grids extending through a soft clay layer to an underlying dense sand. Strong shaking

caused localized shear and tensile cracks over the full height of the DM grid, but the lateral stiffness of the grid did not appear to have been significantly degraded. In addition, rocking of a structure on its shallow footing caused extensive local crushing in the soil-cement at the top of the DM grid for one case. This local crushing was accompanied by greater footing settlements, but the DM grid was still able to maintain vertical load carrying capacity (i.e., the soft clay did not have sufficient strength to support the structure on its own). Three-dimensional nonlinear analyses with pseudo-static loading showed that the rocking foundations produced stress concentrations at the corners of the DM grids, and that simple design equations that allow for those stress concentrations were able to differentiate between the models that did and did not have extensive damage at the tops of the grids. Koseki et al. (2008) examined various factors affecting tensile and shear properties of cement-treated sand and the initiation and propagation of localizations within test specimens; the implications of shear and tensile damage to soil-cement grids was examined through the 3D numerical analyses previously described in Namikawa et al. (2007). Three-dimensional analyses of DM treatments and various lessons learned have also been described in Hasheminezhad and Bahadori (2019), Rostami et al. (2018), and Tong et al. (2019). These various studies collectively illustrate that the design of complex DM configurations for protecting overlying structures increasingly relies on nonlinear 2D or 3D analyses.

## **CENTRIFUGE AND NUMERICAL MODELING FOR AN EMBANKMENT**

Results of a dynamic centrifuge model test and associated 2D nonlinear dynamic analyses of an embankment on a liquefiable foundation layer treated with soil-cement walls are used in this section to illustrate several issues and challenges. The centrifuge tests and nonlinear dynamic analysis procedures are described in detail in Boulanger et al. (2018). This section provides a brief overview of the model tests and analysis procedures, followed by additional analyses examining the role of strain softening in the soil-cement walls.

The centrifuge model, performed on a 9-m radius centrifuge, corresponded to a 28-m tall embankment underlain by a 9-m thick saturated loose sand layer (prototype units) as shown in Fig. 20. Soil-cement walls were positioned through the loose sand layer near the toe of the embankment and covered with a berm. The model was shaken three times with a scaled earthquake motion modified from a recording in the 1995 Kobe earthquake; the peak horizontal base accelerations (PBA) were 0.05 g, 0.26 g, and 0.54 g, respectively. The latter two events liquefied the loose sand layer. Crack sensors in the soil-cement walls showed that they developed limited cracking in the 0.26 g shaking event but sheared through their full length in the 0.54 g event. Cracking and shearing in the soil-cement walls followed irregular complex patterns that varied between walls, as shown by the photographs in Fig. 21 taken during model dissection after testing.

Two-dimensional nonlinear dynamic analyses of the centrifuge test were performed using the finite difference program FLAC (Itasca 2016) and the user-defined constitutive model PM4Sand (Ziotopoulou and Boulanger 2016, Boulanger and Ziotopoulou 2017) for the sands. The treatment zone was modeled as a Mohr Coulomb material with area-averaged composite properties, with the soil-cement assigned a shear strength equal to 80% of its measured peak shear strength. This modeling approach for the soil-cement treatment zone does not simulate strain softening, but rather includes a 20% reduction to account for post-peak strength reductions due to damage during shearing. The results of the numerical simulations were in reasonable agreement with the recorded dynamic responses, including the triggering of liquefaction in the loose sand layer during the PBA = 0.26 g and 0.54 g events. The simulations reasonably approximated the recorded time histories of excess pore pressure, acceleration, and embankment displacements. Parametric analyses illustrated the effects of varying the shear strength of the soil-cement, the procedures for modeling tensile yielding of the soil-cement, the cyclic strength of the loose sand layer,

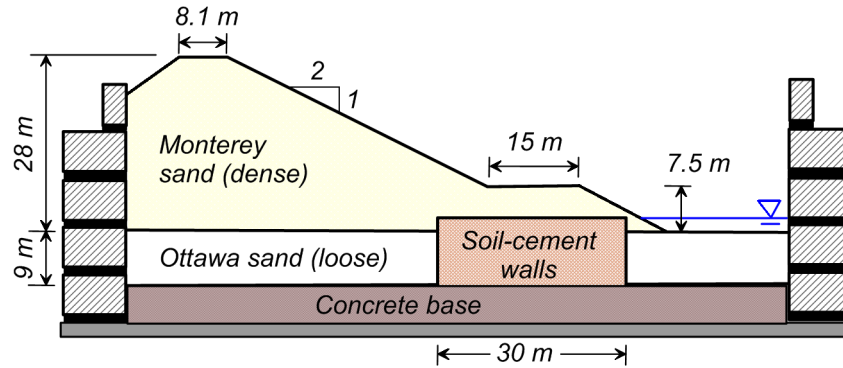


**Fig. 20. Cross-section of centrifuge model showing prototype dimensions (Boulanger et al. 2018)**



**Fig. 21. Post-test excavation photos of soil-cement panels; toe of berm is to left side of the photos (Boulanger et al. 2018)**

and the dynamic loading history. The results of these comparisons provided support for the use of these numerical modeling procedures, including the representation of a treatment zone with area-weighted, non-strain-softening, composite properties, for analyses of embankment dams with soil-cement treatment of liquefiable soils in their foundations.

Additional analyses that simulate strain softening in the soil-cement treatment zone are presented herein to illustrate how they can affect deformation patterns and magnitudes. These simulations used the identical input parameters and procedures as used for the baseline analyses in Boulanger et al. (2018), except for the representation of the soil-cement treatment zone. In one set of analyses, the soil-cement treatment zone is represented using the strain-softening Mohr Coulomb model available with FLAC, wherein the cohesion term (with friction and dilation angles equal to zero) degrades linearly with cumulative plastic shear strain; the cohesion is set to degrade from its peak shear strength to 60% of its peak shear strength at a cumulative plastic shear strain of 10%. The liquefied soil between the soil-cement walls is assumed to have negligible contribution to the composite shearing resistance of the treatment zone. The resulting composite shear resistance versus shear strain for the treatment zone is shown in Fig. 22. For comparison, other analyses are presented using non-strain-softening properties with the treatment zone strength based on either 60% or 100% of the peak soil-cement shear strength (Fig. 22). All three simulations were in reasonable agreement with measured time histories for excess pore pressures and accelerations throughout the model in both stronger shaking events, such that the following discussion focuses on the deformations.

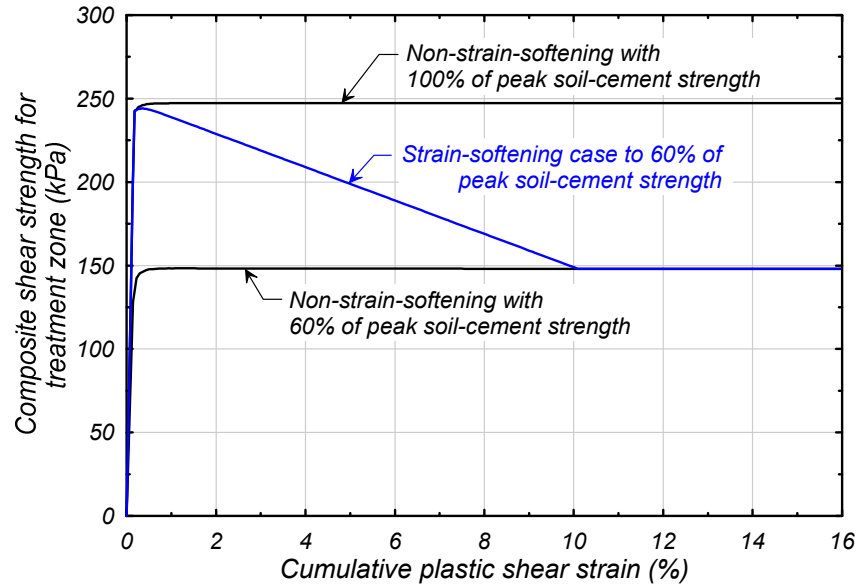


**Fig. 22. Stress-strain responses for composite models of the treatment zone with and without strain softening**

Simulated and measured displacements for the embankment crest and berm during the Kobe 0.26 g shaking event are shown in Fig. 23. The measured displacements are from displacement transducers mounted on racks positioned across the top ring of the container, which moves horizontally relative to the container base during dynamic shaking. The simulation results for the horizontal displacements are therefore also presented as relative to the top container ring. The simulation results using the strain-softening model (red lines) are in close agreement with the measured crest settlement and berm horizontal displacement. The simulation results for the non-strain-softening model with 100% of the soil-cement peak strength significantly under-estimated the berm horizontal displacement and slightly underestimated the crest settlement. The simulation results for 60% of the soil-cement peak strength significantly over-estimated the berm horizontal displacement but reasonably estimated the crest settlement. These results, consistent with those in Boulanger et al. (2018), show that the berm displacement is more sensitive to the treatment zone properties than the crest settlement is.

Deformed meshes with contours of engineering shear strain after the Kobe 0.26 g shaking event are shown in Fig. 24 for two of the above cases: (a) the non-strain-softening model with 60% of the soil-cement peak strength, and (b) the strain-softening model. The analyses using the non-strain-softening model produced slightly greater shear strains in the lower portions of the treatment zone (Fig. 24a), consistent with it producing larger berm horizontal displacements. Note that shear strains in the bottom two rows of zones (or elements) in the treatment zone are comparable for this non-strain-softening case. The analyses using the strain-softening model had slightly smaller shear strains in the treatment zone (Fig. 24b), but the strains were now largely concentrated within the lowest row of zones (or elements). The concentration of shear strains within a single row of zones is expected for a strain-softening model, which also introduces a mesh dependency to the simulations. The shear strains in the localized zone were about 12%, which indicates that these zones likely degraded to their fully damaged shearing resistance near the end of strong shaking (i.e., comparing these strains to the stress-strain responses in Fig. 22). These strains are consistent with the berm horizontal displacement time histories for the strain-softening model being about halfway between the results for the non-strain-softening models with 60% and 100% of the soil-cement peak strength (Fig. 23).

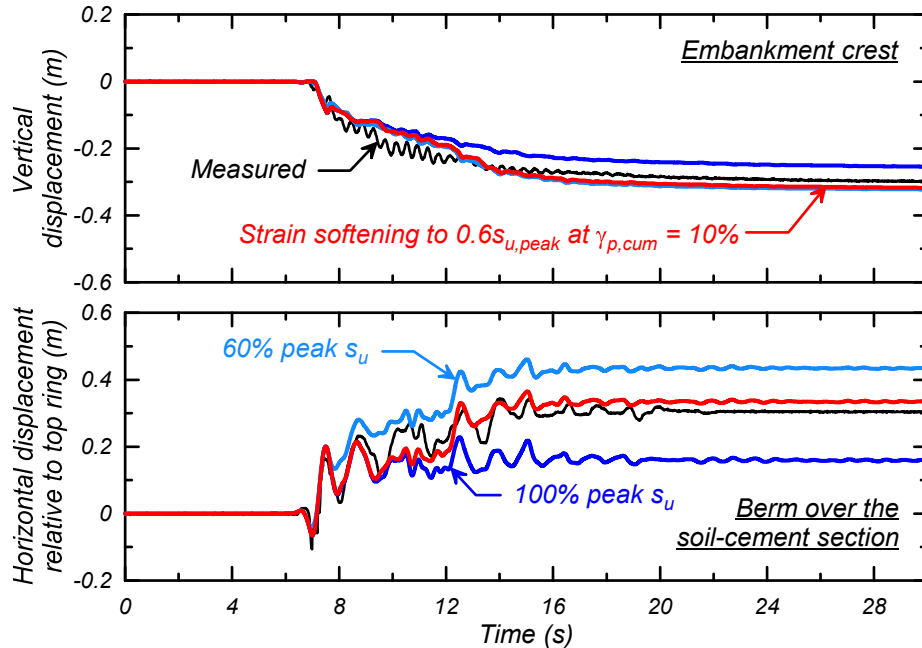


**Fig. 23. Measured and computed displacements for the Kobe 0.26 g event with alternative strength representations for the treatment zone: (a) embankment crest settlement, (b) berm horizontal displacement**

Simulated and measured displacements for the embankment crest and berm during the Kobe 0.54 g shaking event are shown in Fig. 25. The simulation results using the strain-softening model (red lines) overestimate the crest settlement but are in close agreement with the berm horizontal displacement. The simulation results for the non-strain-softening model with 100% of the soil-cement peak strength significantly underestimated the berm horizontal displacement, but slightly overestimated the crest settlement. The simulation results for 60% of the soil-cement peak strength overestimated the berm horizontal displacement and crest settlement. As for the Kobe 0.26 g event, the computed berm displacement is more sensitive to the treatment zone properties than the crest settlement is.

Deformed meshes with contours of engineering shear strain after the Kobe 0.54 g shaking event are shown in Fig. 26 for the same two cases: (a) the non-strain-softening model with 60% of the soil-cement peak strength, and (b) the strain-softening model. The analyses using the non-strain-softening model produced shear strains of 20–40% over the lower four rows of zones in the treatment zone (Fig. 26a), whereas analyses using the strain-softening model produced shear strains of over 60% concentrated in the bottom row of zones in the treatment zone (Fig. 26b). The difference in shear strain patterns in the treatment zone is greater for these two cases than was evident for the Kobe 0.26 g event, in part because the global embankment deformations are much greater. The large shear strains in the localized zone indicate that these zones degraded to their fully damaged shearing resistance early in strong shaking, and yet the differences in shearing resistance early in strong shaking still had a significant effect on berm displacements (Fig. 25).

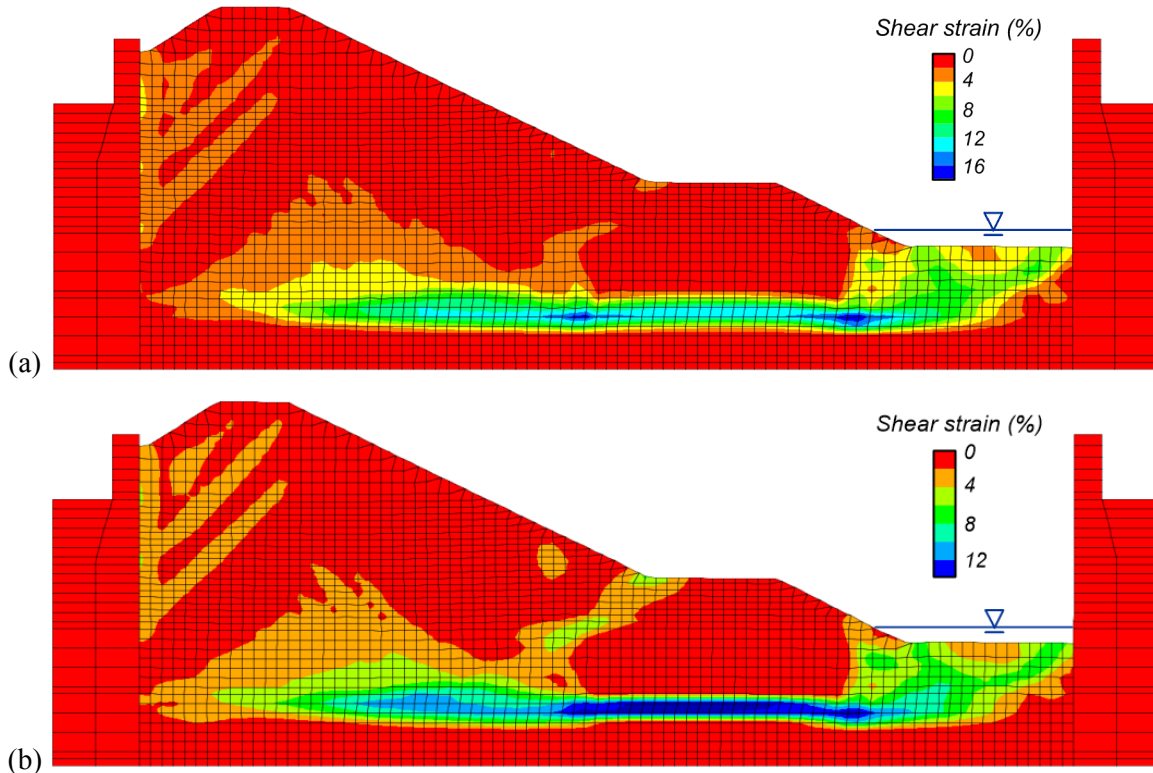


**Fig. 24. Contours of shear strain after shaking for the simulation of the Kobe 0.26 g event: (a) non-strain-softening soil-cement with assigned strength equal to 60% of the true peak strength, and (b) strain-softening soil-cement with strength degrading to 60% of peak strength over 10% cumulative plastic shear strain**

These numerical simulations do not account for a number of complex mechanisms in the treatment zone. Excavation of the centrifuge model showed that the enclosed liquefied sand displaced relative to the soil-cement walls (i.e., extruding between the walls) by amounts that varied across the width of the container and along the length of the walls (Boulanger et al. 2018). The soil-cement walls developed irregular cracking and offsets that varied along the length of the walls and between adjacent walls (Fig. 21). Offsets along these undulating crack surfaces were likely accompanied by local fluctuations in normal stress, which would contribute to changes in excess pore pressure beyond those due to shearing alone. The average excess pore pressures in the soil-cement during shearing would be expected to be less than in the adjacent liquefied sand. Excess pore pressures in the enclosed liquefied sand would diffuse into the cracks in the soil-cement walls during strong shaking, which would reduce the mobilized shear resistance in the walls. The rate of pore pressure diffusion into these cracks would depend on the soil's hydraulic conductivity, the aperture of the wall cracks, the wall thickness, and the difference in pore pressures between the soil and wall materials. In addition, the shear resistance provided by the walls would be expected to degrade progressively during shaking as the cracks grow and develop offsets.

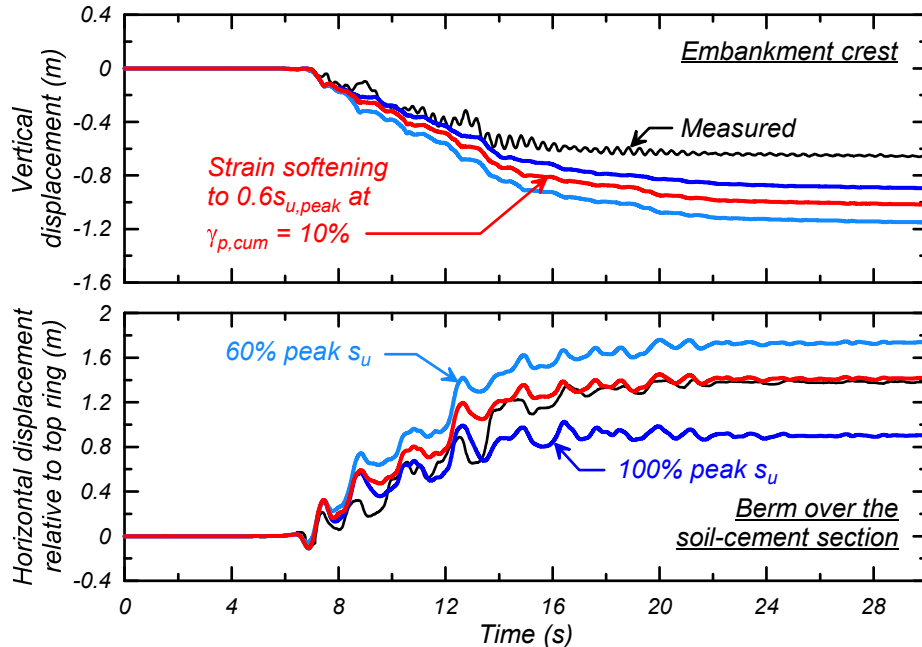


**Fig. 25. Measured and computed displacements for the Kobe 0.54 g event with alternative strength representations for the treatment zone: (a) embankment crest settlement, (b) berm horizontal displacement**

The seismic performance of soil-cement walls in the field may also be affected by details not represented in the centrifuge or numerical models. Soil-cement walls in the field often include longitudinal connecting walls to form a grid or set of grids with intermittent spaces between them to avoid fully impeding ground water flow. The longitudinal walls should reduce the extrusion of liquefied soils between the transverse walls, which could reduce overall deformations. Vertical joints in soil-cement walls constructed as overlapping columns have a smaller chord area ratio compared to the average area ratio for horizontal planes. Yielding along these vertical joints due to their lower area ratio or possibly lower shear strengths would be expected to reduce the lateral stiffness and strength of the wall system.

The detailed responses of soil-cement walls that develop extensive damage during strong shaking are too complex to simulate directly in most practical applications, and hence it is common to use simpler equivalent composite system models with conservative selections for the input parameters/strengths. The good agreement between 2D numerical simulations and measured centrifuge model responses in both Boulanger et al. (2018) and herein suggest that equivalent composite system models may be a reasonable approximation for the type of embankment examined.

It is currently not feasible to perform field dynamic tests to directly evaluate the in-situ performance of a DM treatment for liquefaction mitigation under design seismic loads. Static load tests on DM elements, while useful, do not address the issues associated with liquefaction, ground deformation, or DM-soil dynamic interaction during seismic loading.

Thus, 2D and 3D numerical analysis methods with various levels of sophistication are essential for validating seismic designs and further evaluating the complex mechanisms affecting seismic performance of DM treatments for liquefaction mitigation. Continued development of numerical simulation procedures is needed and would benefit from further physical model testing and improved instrumentation at field sites (e.g., inclinometer casings in the soil-cement walls, between the walls, and outside the treatment areas) to enable gathering key data in future earthquakes.

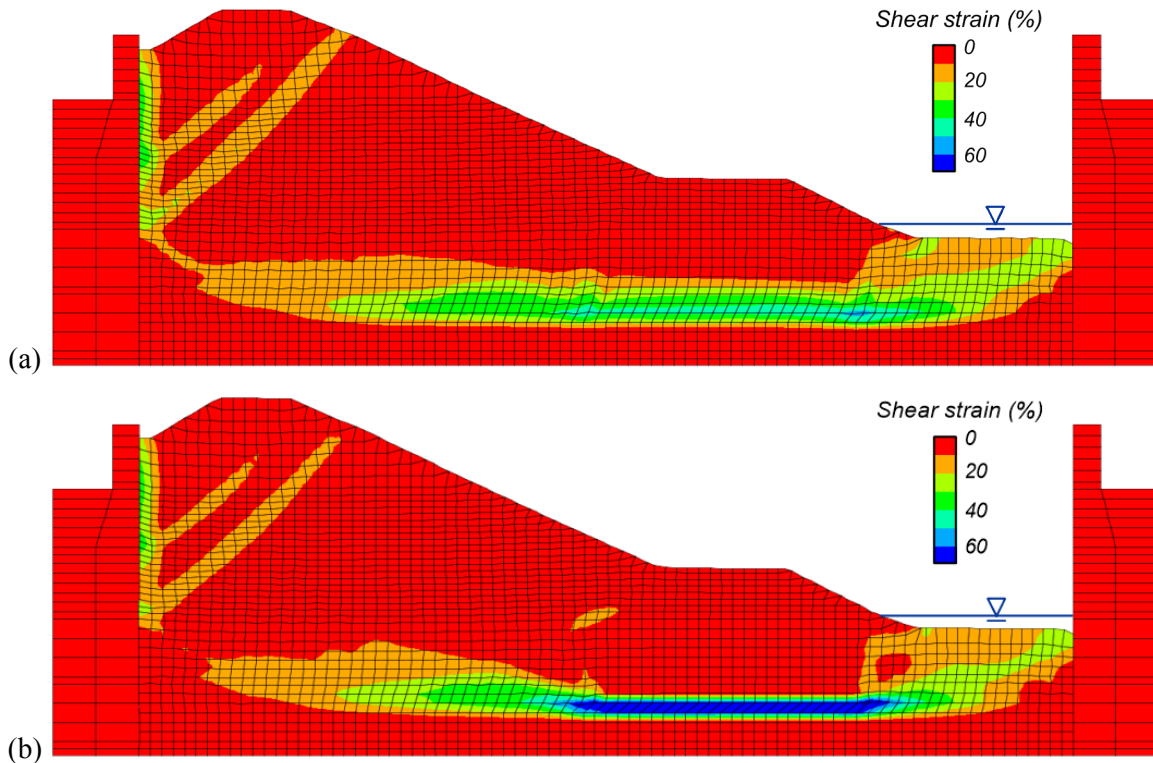


**Fig. 26. Contours of shear strain after shaking for the simulation of the Kobe 0.54 g event: (a) non-strain-softening soil-cement with assigned strength equal to 60% of the true peak strength, and (b) strain-softening soil-cement with strength degrading to 60% of peak strength over 10% cumulative plastic shear strain**

## WEST DOWLING ROAD OVERCROSSING CASE HISTORY

The West Dowling Road Overcrossing in Anchorage, Alaska experienced strong shaking during the November 30, 2018  $M_w=7.1$  earthquake NNW of Anchorage. The subsurface conditions, stability analyses, and design and construction of DM improvements for the abutments of this road overcrossing are described in detail in Yamasaki et al. (2015). This paper reviews the background for this road overcrossing, followed by a summary of its performance during the 2018 earthquake.

### *Overcrossing and subsurface conditions*

The Alaska Department of Transportation and Public Facilities (Alaska DOT&PF) built the West Dowling Road Overcrossing in Anchorage, Alaska in 2014. It is a single-span, steel box girder bridge approximately 61 m long and 30 m wide. It carries West Dowling Road over both Arctic Boulevard and double tracks of the Alaska Railroad. The approach embankments are about 12 m high on both sides of the overcrossing. The cantilever-type abutments are supported on shallow footings, each about 7.3 m wide by 38 m long, and the approach fills are retained by mechanically-stabilized earth (MSE) walls. The photographs in Figs. 27 and 28 show the overcrossing during construction.

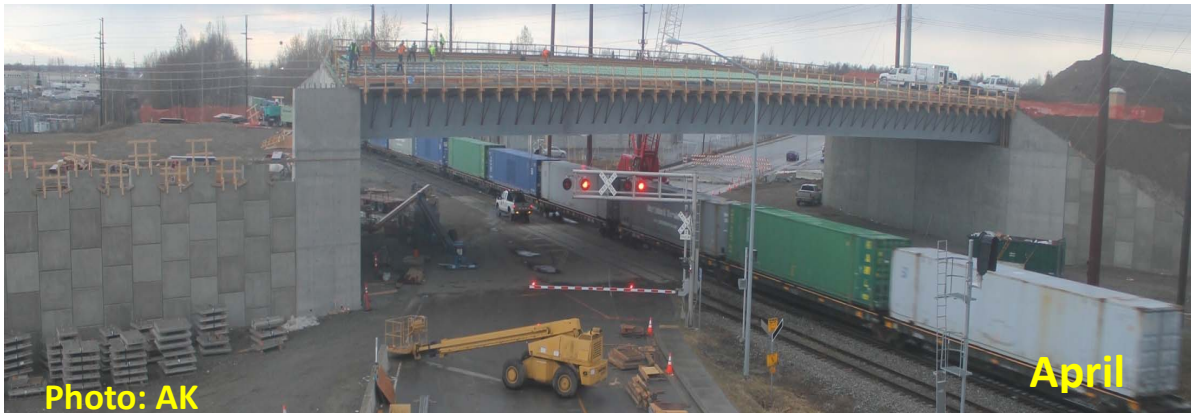


**Fig. 27. West Dowling Road Overcrossing during construction (AK DPT web cam 2015, view looking northwest); note the MSE wing walls on both abutments and the active railroad traffic**



**Fig. 28. West Dowling Road Overcrossing near completion (Photo courtesy of HDR; ©2020); note the spur road crossing under the south approach fill (upper right corner of photograph)**

The subsurface conditions for the abutments are illustrated by the borehole log in Fig. 29. Surficial fill, peat, organic silts, and silts with organics are encountered to depths of about 4.5 m (15 ft), followed by a stratum of soft or loose-to-medium-dense silt to a depth of about 9.0 m (30 ft). These weaker upper soils are in turn underlain by strata of dense silt to about 21 m (70 ft), clay to about 30 m (100 ft), and silt to about 33 m (110 ft). These upper strata were interpreted to be glacially-derived, Holocene sediments. These strata were underlain by dense gravels that were interpreted to be till deposits of Pleistocene age. Bedrock was inferred to be several hundred feet deep. The water table was at a depth of about 3 m (10 ft).

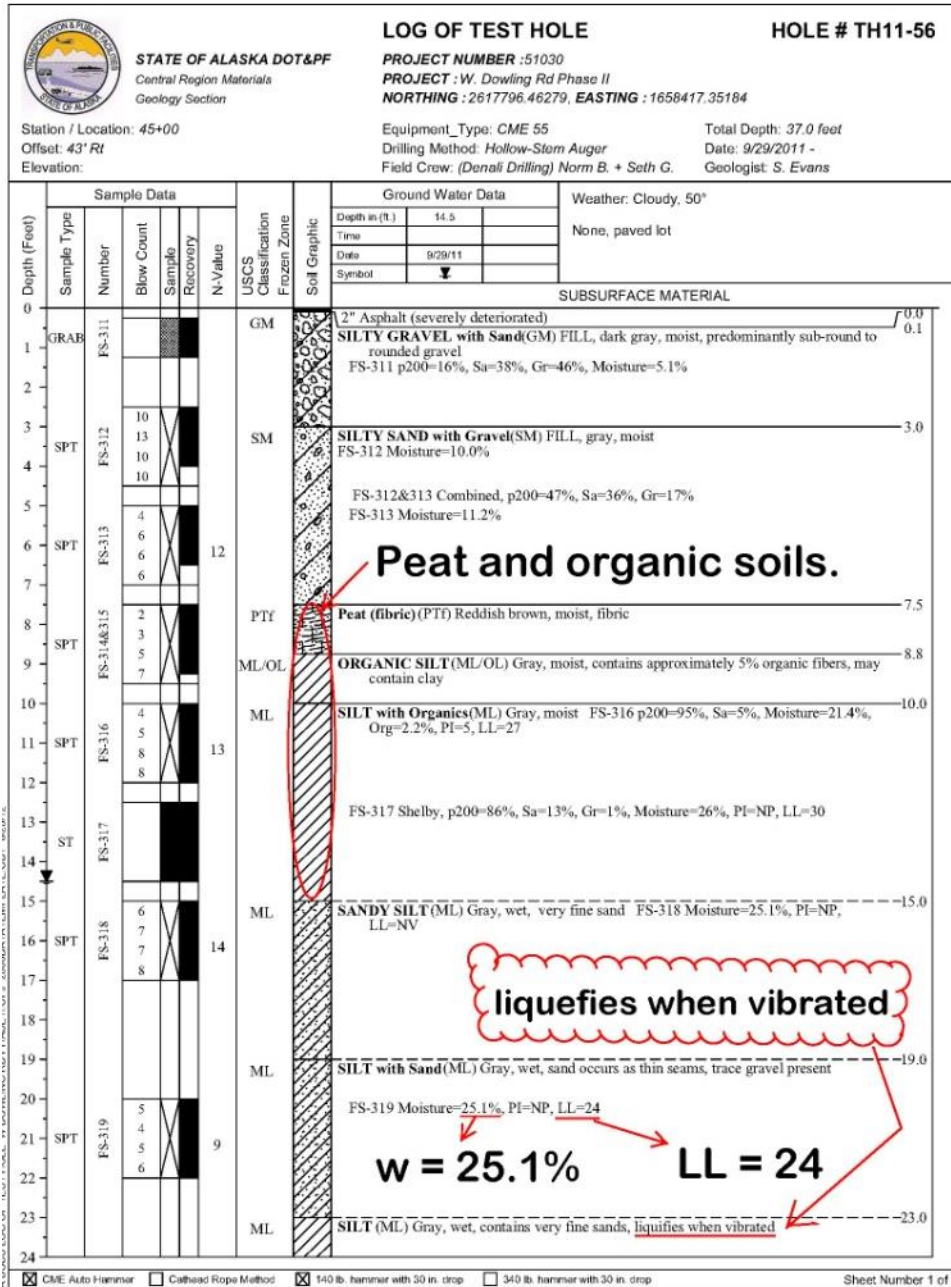


**Fig. 29. Borehole log illustrating subsurface conditions at the West Dowling Road Overcrossing (after Alaska DOT&PF 2011)**

The soft peat, organic silts, and silts in the upper 9 m were problematic due to their low strengths and potential for liquefaction-induced strength loss during earthquake loading. The upper 3–4.5 m of peat and organic silts were excavated and replaced with granular fill. The underlying silt stratum (to depths of about 9 m) was generally non-plastic to low-plasticity with water contents of 25–30% and uncorrected SPT N values ranging from about 5 to 15. Tests on a composite sample of this material from four borings gave a liquid limit (LL) of 23, plasticity index (PI) of 4, fines content of 71%, and a USCS classification of CL-ML. These data suggest the liquidity index for this silt was generally close to or greater than unity, which indicates a relatively high potential for earthquake-induced strength loss.

A liquefaction evaluation was performed for  $M = 9.2$  megathrust earthquake at a distance of 55 km producing a peak ground acceleration of 0.27 g. The liquefaction analysis, using the simplified procedure with the recommendations by Youd et al. (2001), indicated that most of the silt stratum between depths of about 6 and 9 m was expected to liquefy. The silt was assigned a post-liquefaction residual shear strength of 19 kPa (400 psf) for evaluating stability of the abutments. This strength estimate was reduced from the 29 kPa (600 psf) estimate obtained using the relationships by Seed and Harder (1990) and Stark and Mesri (1992) because the abutments are sensitive to deformations and relatively large shear strains would be required to mobilize the full residual shear strength. Limit equilibrium slope stability analyses subsequently indicated that the overcrossing abutments would be unstable with a post-liquefaction static factor of safety of about 0.80.

### ***Design and construction of DM improvements***

An evaluation of foundation alternatives led to the selection of DM improvement zones beneath both abutments, along with the overcrossing being supported on shallow foundations. Other alternatives that were evaluated included deep foundations and vibro-displacement stone columns. Deep mixing was selected for three reasons: (i) it can be used close to sensitive structures like the railroad tracks and underground utilities, (ii) it was the most cost effective, and (iii) it would not require post-treatment densification verification testing. The objectives of the DM improvements were to strengthen the foundation and protect the abutments from earthquake-induced deformations, allow the bridge abutments to be supported by shallow foundations, and reduce static settlements for the abutments.

The DM treatment configurations for both abutments are shown in Fig. 30, including the plan view layout and a cross-section through an abutment. Deep mixed columns with diameters of 2.44 m (8 ft) were overlapped to form shear panels aligned longitudinally with the roadway. The columns/panels were spaced to produce an  $A_r$  of about 90% beneath the abutment footings and about 50% in the area surrounding the footings. The  $A_r = 50\%$  area extends about 10.7 m in front of the abutment footings and about 9 m beyond the other sides of the footings. The columns were constructed from a working surface at an elevation of about 32 m (104 ft) after excavation of the surficial fill, peat, and organic soils (see section A-A in Fig. 30). Columns were constructed by first predrilling to a depth of about 2.4 m (8 ft), followed by soil mixing with a 2.44-m diameter mixing tool to a depth of about 6 m, such that columns were founded in the underlying dense silt layer. Compacted aggregate base course, about 1.8 m thick, was placed on top of the DM columns beneath the abutment footings as the load transfer platform (Fig. 30).

The specified value for the average unconfined compressive strength ( $q_u$ ) of the soil-cement, obtained from testing of wet-grab field samples, was 1.0 MPa (150 psi), from which the design  $q_u$  value for the in-situ soil-cement was 0.69 MPa (100 psi). The design shear strength ( $s_{dm}$ ) for the in-situ soil-cement was taken as 80% of  $q_u/2$  or about 275 kPa (40 psi). The composite shear strength of the improved ground was estimated based on the assumption that native soil between columns/panels provided no shearing resistance. Limit equilibrium slope stability analyses indicated the post-earthquake (post-liquefaction) static factor of safety was increased to 1.77 with the DM treatments.

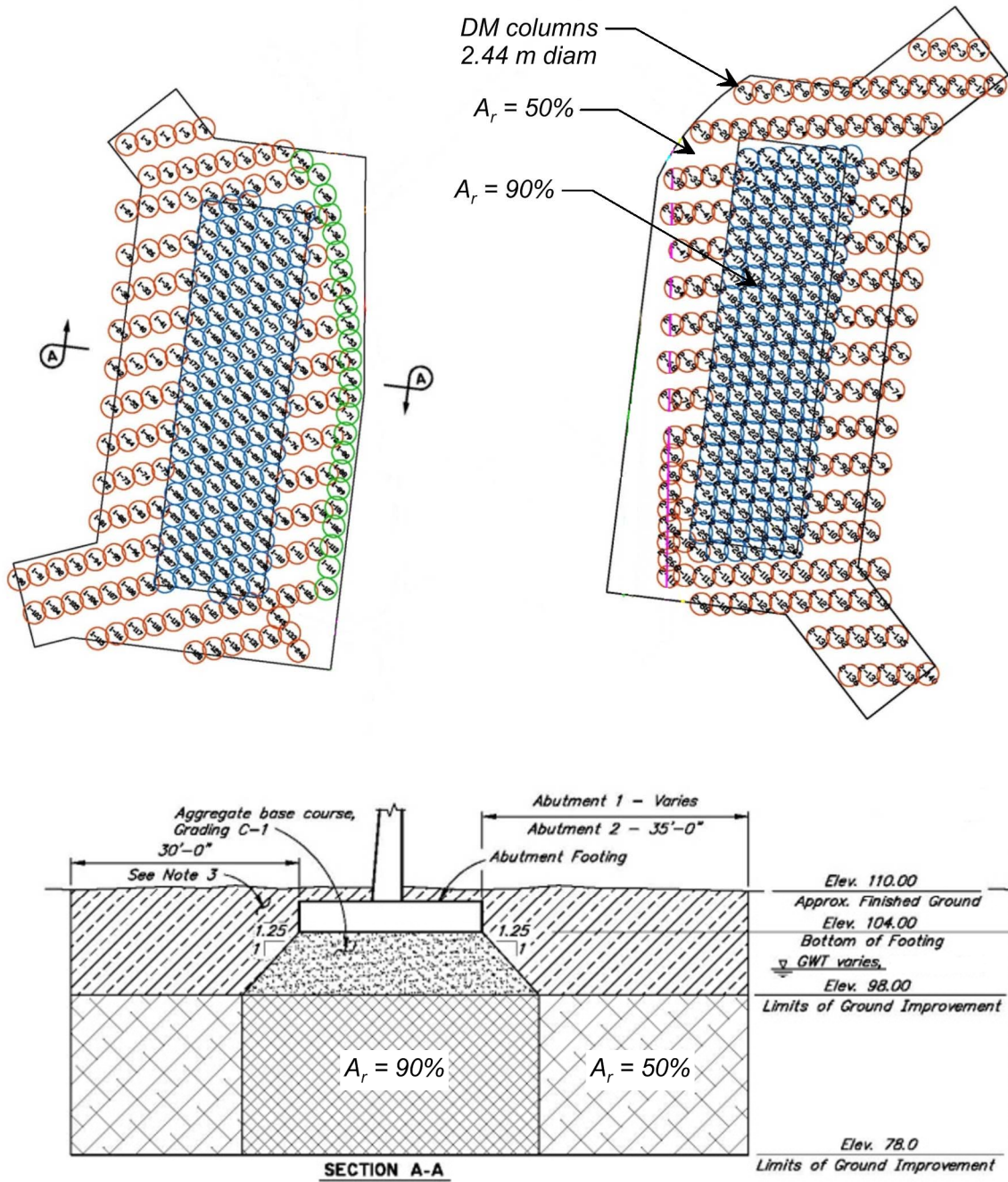


**Fig. 30. Deep-mixing plan (top) and cross-section A-A (bottom) for West Dowling Road Overcrossing (modified from Alaska DOT&PF 2013, Yamasaki et al. 2015)**

Pre-production laboratory mix design tests used a composite sample of the silt layer mixed with cement slurry at different binder contents and cast into 75-mm diameter by 150-mm high cylinders and cured for testing at 3, 7, 14, 21, 28, and 56 days. The increase of  $q_u$  with specimen age for three binder contents in-place (ratio of dry weight of binder to the combined soil and grout volume) is shown in Fig. 31. A binder content (in-place) of  $200 \text{ kg/m}^3$  was selected as the production dosage to achieve the field specified average  $q_u$  of 1.0 MPa at 56 days.

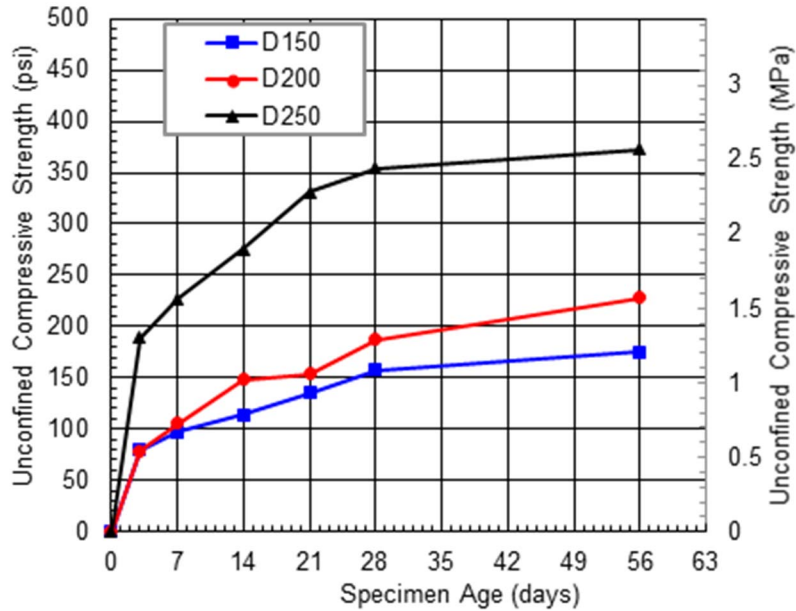


**Fig. 31. Unconfined compressive strength versus specimen age for laboratory soil-cement mixes with binder contents (in place) of 150, 200, and 250 kg/m<sup>3</sup> based on ASTM D 1633**

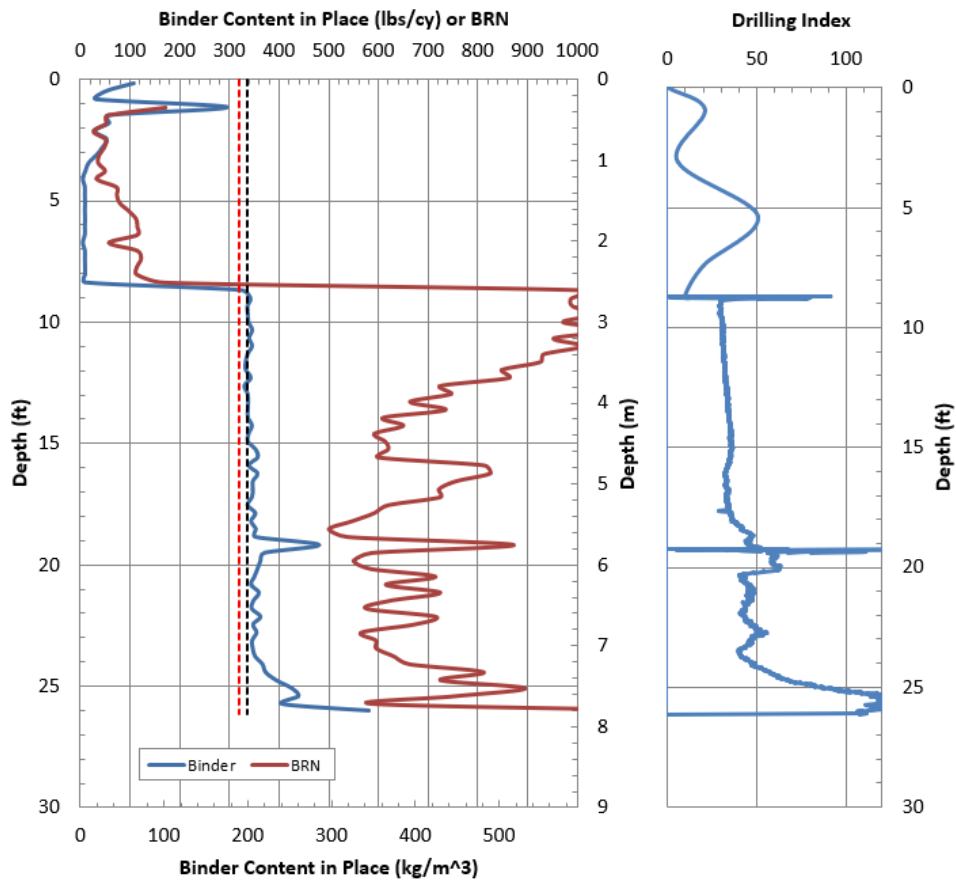
Deep mixing was closely monitored during construction and kept a minimum of 6 m from the active railroad lines (Fig. 32). A data acquisition system (DAQ), as shown in Fig. 33a, was used to monitor and record the mast inclination, mixing rotation speeds, tool depth, penetration/withdrawal rates, grout injection pressure, grout flow rate, density, and volume. In real time, the in-cab computer monitors a variety of mixing parameters and the blade rotation number (number of blade cuts per meter of DM column) as a function of depth, controls the in-place binder content, and graphically displays this information for the operator. In addition, the torque and crowd pressure measurements on the mixed blades were used to compute a Drilling Index (DI) that could be used to estimate the soil strength (Arora et al. 2015), and thus assess whether the columns had reached the dense silt strata (Fig. 33b). All mixing data were wirelessly uploaded to a data server that could be accessed remotely by project engineers.



**Fig. 32. Deep mixing at the west approach abutment; minimum clearance of 6 m between DM columns and the active Alaska Railroad (Yamasaki et al. 2015)**



(a)



(b)

**Fig. 33. Monitoring of deep-mixing process: (a) data acquisition system and operator readouts, and (b) profile of binder content, blade rotation number, and drilling index for one deep-mixed column**

Wet grab samples were obtained by pushing a sampler into freshly completed soil-cement columns at random depths. Samples were screened using a #4 (4.75-mm) sieve and cast into ten cylinders (75-mm diameter, 150-mm height) for testing in pairs after curing for 3, 7, 14, 28, and 56 days (Fig. 34) based on ASTM D1633. Grab samples were obtained from about every seventh column; the total number of grab

samples was 75. The arithmetic average  $q_u$  at 56 days was 2.14 MPa (310 psi), with a sample standard deviation of 0.42 MPa (61 psi) (COV = 20%), as shown in Figs. 35 and 36. The field-installed DM columns' average  $q_u$  was over twice the design average of 1.03 MPa (150 psi), with just 4% of samples exhibiting a UCS less than the design average strength.



Fig. 34. Testing of field samples: (a) wet grab samples, (b) unconfined compression test

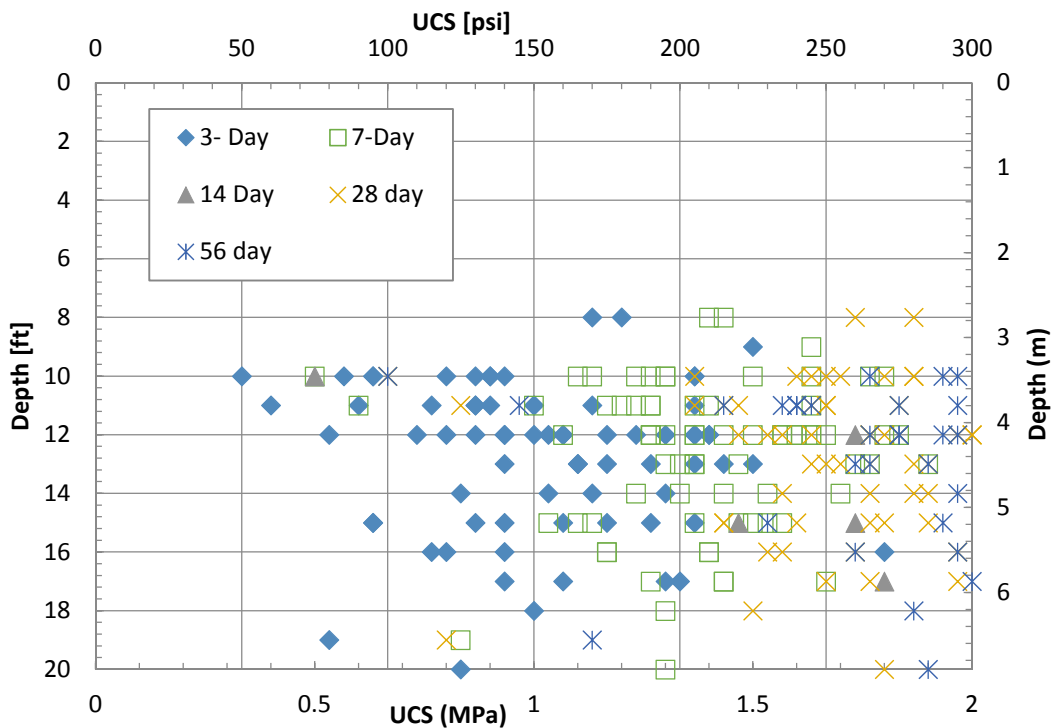
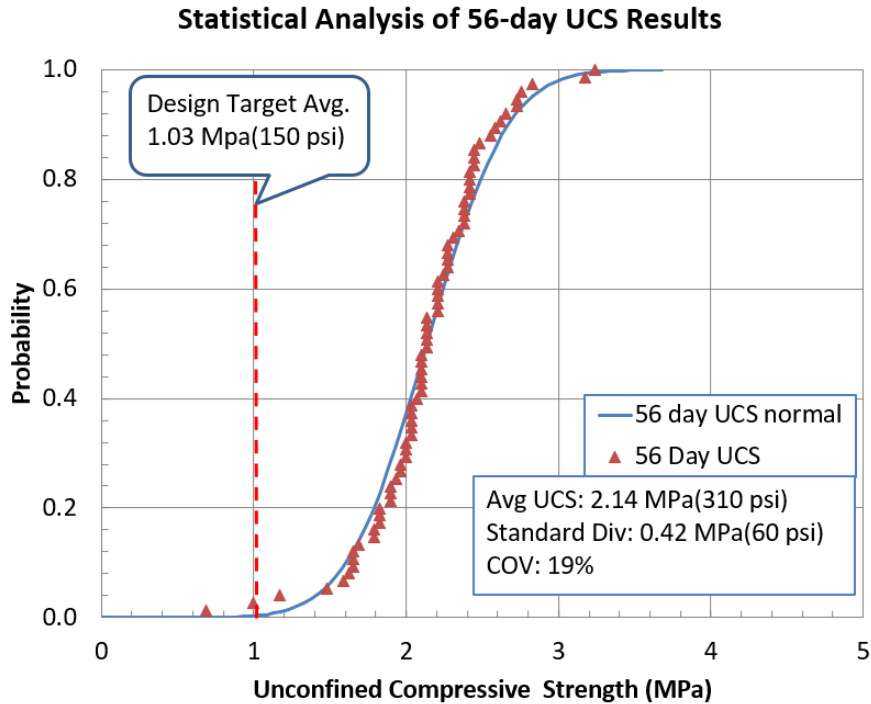


Fig. 35. Unconfined compressive strengths for soil-cement field samples from different depths and for different curing ages



**Fig. 36. Unconfined compressive strengths statistical distribution at 56 days of age**

The DM work was completed in 32 days, followed by construction of the bridge and approach embankments. The railroad and the underground utilities remained in operation throughout construction. The overcrossing opened to public traffic in November 2015.

### ***2018 Anchorage Earthquake***

On November 30, 2018, a magnitude 7.1 earthquake occurred 14 km north-northwest of Anchorage, Alaska, with peak ground accelerations (PGA) of 0.17 g to 0.47 g recorded throughout Anchorage, as shown on the map in Fig. 37. The earthquake caused significant damage in the Anchorage area, including building foundation settlements and roadway embankment failures. The West Dowling Road Overcrossing was inspected by Alaska DOT and remained in normal operation after the earthquake. The overcrossing was also inspected by members of the GEER reconnaissance team on December 10–12, 2018, with support from the DOT. The following is a summary of the observations documented in GEER (2018).

The two strong motion recording stations closest to the West Dowling Road Overcrossing (Fig. 37) were the 8027 State Fish and Game station (about 0.7 km to the southeast), where the PGA was about 0.47 g, and the K208 Anchorage, Spenard Recreation Center station (about 1.8 km to the northwest), where the PGA was about 0.29 g. The COSMOS Virtual Data Center (accessed March 2020) lists the site geology as "soft clay" for the 8027 station and as NEHRP D (stiff soil) for the K208 station. The site conditions at the West Dowling Road Overcrossing appear more consistent with those expected at the 8027 station, which is also the closer station. Thus, the overcrossing is estimated to have experienced a PGA of about 0.35–0.45 g, which is higher than the overcrossing design PGA of 0.27 g.

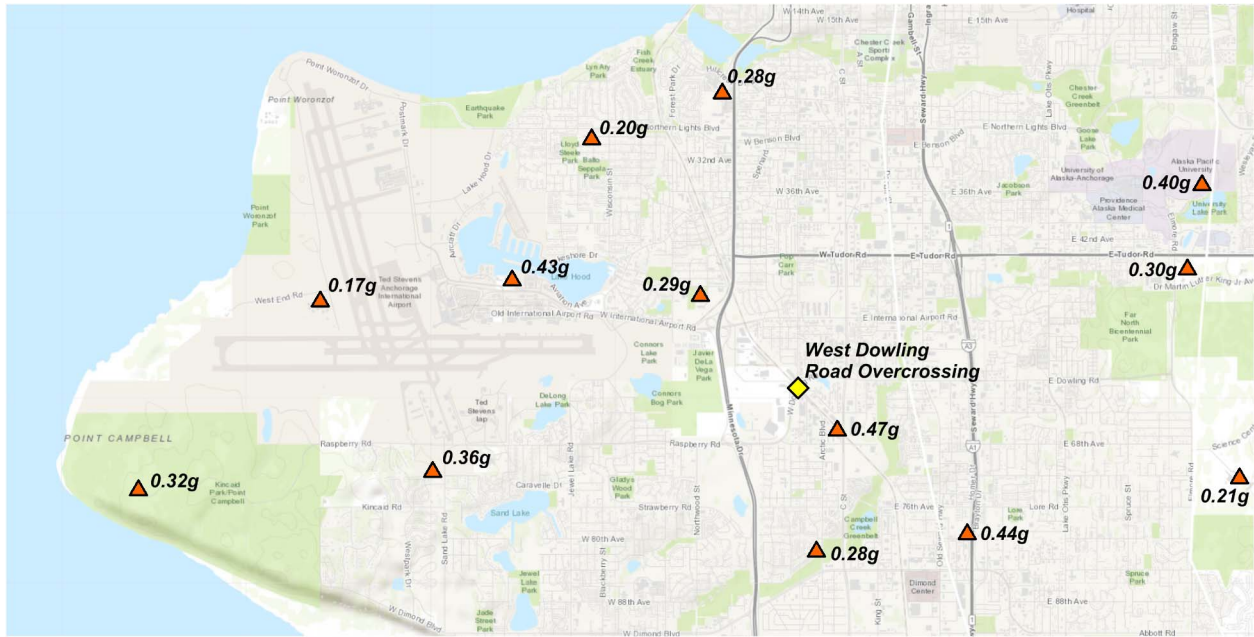


**Fig. 37. Map showing locations of West Dowling Road Overcrossing and strong ground motion stations with the recorded peak ground accelerations during the  $M_w=7.1$  – 14km NNW of Anchorage, Alaska, earthquake of November 30, 2018 (base image and PGA values from USGS ShakeMap, accessed March 2020)**

The road overcrossing (Fig. 38) and approaches performed well during the earthquake, with only light damage to various components (GEER 2018). Minor buckling was observed in guardrails spanning expansion joints and light sections supporting guardrails. Expansion joints along the northeast abutment showed some evidence of pounding with shear cracks and relative permanent displacements of up to 25 mm (Fig. 39). Spalling of concrete was observed for several shear keys along both abutments. Expansion bearings appeared fully extended during AKDOT inspections, which was interpreted as suggesting the abutments may have moved closer together. The southwestern abutment appeared to tilt away from the approach by about 0.4 degrees on the western edge and 1.1 degrees on the eastern edge. The northeastern abutment appeared to tilt away from the approach by zero degrees on western edge and 0.4 degrees on the eastern edge. These tilt measurements were interpreted as being consistent with the full extension of the expansion bearings for the superstructure.



**Fig. 38. West Dowling Road Overcrossing on December 4, 2018 (courtesy of D. Hemstreet; from GEER 2018)**



**Fig. 39. Photographs at the northeast transition from the bridge span to the approach fill showing evidence of possible pounding and permanent transverse displacements (courtesy of D. Hemstreet, from GEER 2018)**

Minor deformations were observed in the MSE wall panels around the culvert tunnel that passes under the approach fill immediately south of the overcrossing bridge, as shown by the set of photographs in Fig. 40 (GEER 2018). The MSE wall panels were observed to have rotated toward the culvert on both sides of the culvert and approach fill. The MSE walls at these locations are outside the DM improvement area. Panel gaps showed evidence of closure and extension movements of up to 75 mm and tilts of up to 4.2 degrees. Several bearing pads were unloaded or loaded depending on the tilting of the wall panels.



**Fig. 40. MSE walls around the culvert tunnel immediately south of the West Dowling Road Overcrossing: close ups illustrate panel movements, panel tilts, and unloading of a bearing pad (GEER 2018)**

The approach fills and abutments showed no evidence of ground failure or large differential soil movements (GEER 2018), except for a minor slip on the southern face of the eastern approach fill (Fig. 41). This slip had crack widths 100 mm wide and a vertical scarp 300 mm high. Planted saplings on this face had inclinations consistent with the observed slope deformations.

The good performance of the West Dowling Road Overcrossing during this  $M_w=7.1$  earthquake shows that the DM improvements under both abutments provided the desired foundation support and helped keep deformations to acceptable levels. The approach embankments on both sides of the overcrossing also performed relatively well despite the absence of DM improvements, which may be partly attributed to the removal and replacement of the weaker soils (surficial fill, peat, and organic soil) in the upper 3–4.5 m, the fact the approach embankments' heights decrease with distance from the overcrossing, the gentle slope, or the soil properties being greater than estimated for design purposes. Future analyses of this case history, using NDA or simplified procedures, would benefit from additional soil characterization data for the soft or loose-to-medium dense silt layer that remained in-place around the DM treatments, and should examine the response of both the overcrossing and the approach embankments. Regardless, this case history provides an example of DM design and construction practices, in addition to favorable performance under strong earthquake loading.



**Fig. 41. Slip on the southern face of the eastern approach fill with cracks up to 100 mm wide and a vertical scarp up to 300 mm high (GEER 2018)**

## CONCLUDING REMARKS

Deep mixing is an effective option for mitigating earthquake-induced liquefaction effects for a wide range of civil infrastructure systems. DM treatments in various configurations can reduce the potential for liquefaction triggering, reduce lateral and vertical ground deformations due to liquefaction in the enclosed or surrounding native soils, and provide support and protection for overlying structures and their foundations. Several issues regarding the design of DM treatments for liquefaction mitigation were reviewed: i.e., general design considerations, liquefiable soil properties, soil-cement properties, prevention of liquefaction triggering with columnar reinforcements, prevention of liquefaction triggering with grid reinforcements, reduction of lateral spreading or embankment displacements, and support and protection of overlying structures and their foundations. The body of experimental and theoretical studies in the literature demonstrate that soil-cement grids or lattices are generally more effective than columns for mitigating liquefaction effects, and that the design of complex DM configurations increasingly utilizes 2D or 3D nonlinear analysis methods.

Results from a dynamic centrifuge model test and associated nonlinear dynamic analyses for an embankment on liquefiable soils treated with soil-cement walls were used to illustrate several challenges and complex behaviors. The centrifuge test identified a number of complex local mechanisms that current nonlinear dynamic analysis methods generally do not account for; e.g., DM cracking patterns and offsets, extrusion of soil between the soil-cement wall panels, and diffusion of excess pore pressures into the soil-cement cracks. Despite these limitations, the generally good agreement between observed and simulated global responses (e.g., crest settlements, berm displacements) with the 2D analysis using equivalent composite modeling for the treatment zone suggests that these analysis approximations may be reasonable for at least the type of embankment examined.

The application of deep mixing to mitigate against liquefaction at the abutments of the West Dowling Road Overcrossing and the subsequent performance of the overcrossing during the 2018  $M_w=7.1$

Anchorage Earthquake were described. The good performance of the overcrossing under strong shaking shows that the DM improvements under both abutments provided the desired foundation support and helped limit deformations to acceptable levels. This case history provides an example of DM design and construction practices, in addition to an example of good performance under strong earthquake loading.

The further advancement of deep mixing for liquefaction mitigation would benefit from the continued development and validation of numerical simulation procedures for soil-cement grid or lattice systems. Large-scale centrifuge model tests are needed to obtain experimental data across a broader range of configurations and loading conditions, so that the validation domain for available numerical simulation procedures is more representative of conditions encountered in practice. In addition, the systematic installation of appropriate instrumentation at treated sites (e.g., inclinometer casings in the soil-cement walls, between the walls, and outside the treatment areas) are needed to increase opportunities for gathering invaluable data in future earthquakes.

## **ACKNOWLEDGMENTS**

The work described in the section "Centrifuge and numerical modeling for an embankment" was supported in part by the Pacific Earthquake Engineering Research Center (PEER) under project number 1120-NCTRB and the California Department of Water Resources (DWR) under Contract 4600009751. Any opinions, findings, or recommendations expressed herein are those of the authors and should not be interpreted as representing the official policies, either expressed or implied, of the above organizations. The deep mixing work at the West Dowling Road Overcrossing had many contributors, including K. Yamasaki, D. Helmstreet, and A. Gerondale. Valuable suggestions and comments regarding different parts of the manuscript were provided by Allen Sehn, Jim Gingery, and David Yang. The authors appreciate the above support and assistance.

## **REFERENCES**

- Arora, S., Shao L., and Conkle C., 2015. Utilizing Real-Time Data and Statistical Analysis for Wet Soil Mixing: A Case Study. DFI Deep Mixing 2015, San Francisco, California.
- Azizian, A., Hall, B.E., and Preece, M.L., 2017. Evergreen line rapid transit project: deep foundation and ground improvement solutions. Proc., NZSEE Conference, New Zealand.
- Baecher G.B., and Christian, J.T., 2003. Reliability and statistics in geotechnical engineering. Chichester: John Wiley and Sons Ltd.
- Baez, J.I., 1995. A design model for the reduction of soil liquefaction by using vibro-stone columns. Ph.D. thesis, University of Southern California.
- Bahmanpour, A., Towhata, I., Sakr, M., Mahmoud, M., Yamamoto, Y., and Yamada, S., 2019. The effect of underground columns on the mitigation of liquefaction in shaking table model experiments. Soil Dynamics and Earthquake Engineering, 116(2019), 15–30.
- Barron, R.F., Kramer, C., Herlache W.A., Wright, J., Fung, H., and Liu, C., 2006. Cement deep soil mixing remediation of Sunset North Basin Dam. Dam Safety 2006, ASDSO.
- Bouckovalas, G.D., Papadimitriou, A.G., Kondis, A., and Bakas, G.J., 2006. Equivalent-uniform soil model for the seismic response analysis of sites improved with inclusions. Proc., 6th European Conf. on Numerical Methods in Geotechnical Engineering, Taylor & Francis, London, 801–807.

Boulanger, R.W., and Ziotopoulou, K., 2017. PM4Sand (Version 3.1): A sand plasticity model for earthquake engineering applications. Report No. UCD/CGM-17/01, Center for Geotechnical Modeling, Department of Civil and Environmental Engineering, University of California, Davis, CA.

Boulanger, R.W., Khosravi, M., Khosravi, A., and Wilson, D.W., 2018. Remediation of liquefaction effects for an embankment using soil-cement walls: Centrifuge and numerical modeling. *Soil Dynamics and Earthquake Engineering*, 114(2018), 38–50, 10.1016/j.soildyn.2018.07.001.

Boulanger, R.W., Munter, S.K., Krage, C.P., and DeJong, J.T., 2019. Liquefaction evaluation of interbedded soil deposit: Çark Canal in 1999 M7.5 Kocaeli Earthquake. *Journal of Geotechnical and Geoenvironmental Engineering*, ASCE, 145(9): 05019007, 10.1061/(ASCE)GT.1943-5606.0002089.

Bradley, B.A., Araki, K., Ishii, T., and Saitoh, K., 2013. Effect of lattice-shaped ground improvement geometry on seismic response of liquefiable soil deposits via 3-D seismic effective stress analysis. *Soil Dynamics and Earthquake Engineering*, 48(2013), 35–47.

Bray, J.D., Boulanger, R.W., Cubrinovski, M., Tokimatsu, K., Kramer, S.L., O'Rourke, T., Rathje, E., Green, R.A., Robertson, P.K., and Beyzaei, C.Z., 2017. U.S.-New Zealand-Japan International Workshop, Liquefaction-induced ground movement effects. PEER Report 2017/02, Pacific Earthquake Engineering Research Center, University of California, Berkeley, CA.

Bruce, D.A., 2001. An Introduction to the Deep Mixing Methods as Used in Geotechnical Applications, Volume III: The Verification and Properties of Treated Ground, FHWA-RD-99-167, Federal Highway Administration, October 2001.

Bruce, M.E., Berg, R.R., Filz, G.M., Collin, J.G., Terashi, T., and Yang, D.S., 2013. FHWA Design Manual: Deep Mixing for Embankment and Foundation Support. FHWA-HRT-13-04. Federal Highway Administration, Washington DC.

Chai, J., Shrestha, S., and Hino, T., 2019. Failure of an Embankment on Soil-Cement Column-Improved Clay Deposit: Investigation and Analysis. *Journal of Geotechnical and Geoenvironmental Engineering*, 145(9): 05019006, DOI: 10.1061/(ASCE)GT.1943-5606.0002118.

Christie, S., Zhang, Y., Dickenson, S., and Pitner, B., 2019. Seismic analysis and ground improvement design for the PCT Marine Terminal at the Port of Alaska. *Ports 2019: Port Engineering*, P. Jain and W. S. Stahlman III, eds., 538–549, DOI: 10.1061/9780784482612.

Coastal Development Institute of Technology, 2002. *The Deep Mixing Method: Principle, Design, and Construction*. Edited by Coastal Development Institute of Technology (CDIT), Japan. A. A. Balkema Publishers, Lisse, The Netherlands.

Cubrinovski, M., and Ishihara, K., 1998. State concept and modified elastoplasticity for sand modelling. *Soils and Foundations*, 38(4), 213–225.

Cubrinovski, M., and Robinson, K., 2016. Lateral spreading: Evidence and interpretation from the 2010–2011 Christchurch earthquakes. *Soil Dyn. Earthq. Eng.*, 91, 187–201, DOI: 10.1016/j.soildyn.2016.09.045.

Darby, K.M., Boulanger, R.W., and DeJong, J.T., 2019. Effect of partial drainage on cyclic strengths of saturated sands in dynamic centrifuge tests. *Journal of Geotechnical and Geoenvironmental Engineering*, ASCE, 145(11): 04019089, DOI: 10.1061/(ASCE)GT.1943-5606.0002085.

Demir, S., and Ozener, P., 2019. Numerical investigation of seismic performance of high modulus columns under earthquake loading. *Earthquake Engineering and Engineering Vibration*, 18(4): 811–822, DOI: 10.1007/s11803-019-0537-2.

Demir, S., and Ozener, P., 2020. Parametric investigation of effectiveness of high modulus columns in liquefaction mitigation. *Soil Dynamics and Earthquake Engineering*, 139(2020), 106337, DOI: 10.1016/j.soildyn.2020.106337.

Durgunoglu, H.T., 2006. Utilization of high modulus columns in foundation engineering under seismic loadings. U.S. 8th National Conf. on Earthquake Engineering, Earthquake Engineering Research Institute, San Francisco.

EBMUD, 2020. Chabot Dam Upgrade, East Bay Municipal Utility District, <https://www.ebmud.com/about-us/construction-and-maintenance/construction-my-neighborhood/chabot-dam-upgrade/>, accessed July 1.

Elgamal, A., Lu, J., and Forcellini, D., 2009. Mitigation of liquefaction-induced lateral deformation in a sloping stratum: Three-dimensional numerical simulation. *J. Geotechnical and Geoenvironmental Engineering*, 135(11), 1672–1682, DOI: 10.1061/(ASCE)GT.1943-5606.0000137.

Filz, G.M., and Navin, M.P., 2006. Stability of Column-Supported Embankments. Report No. VTRC 06-CR13, Virginia Transportation Research Council, Charlottesville, Virginia.

Filz, G.M., and Navin, M.P., 2010. A Practical Method to Account for Strength Variability of Deep-Mixed Ground. *GeoFlorida 2010: Advances in Analysis, Modeling & Design*, Geotechnical Special Publication 199, 2426–2433, American Society of Civil Engineers, Reston, VA.

Filz, G.M., Adams, T., Navin, M.P., and Templeton, A.E., 2012. Design of deep mixing for support of levees and floodwalls. *Proc., 4<sup>th</sup> International Conference on Grouting and Deep Mixing*, ASCE Geotechnical Special Publication, GSP 228, 89–133.

Filz, G.M., Reeb, A., Grenoble, A., and Abedzadeh, F., 2015. Material Properties for Analysis of Deep Mixing Support Systems. *Proc. Deep Mixing 2015 Conf.*, Deep Foundations Institute, Hawthorne, NJ, 823–834.

Friesen, S., and Balakrishnan, A., 2012. General approach used for the seismic remediation of Perris Dam. *Proc. 32nd Annual USSD Conference*, United States Society on Dams.

GEER, 2018. Geotechnical Engineering Reconnaissance of the 30 November 2018 M7.0 Anchorage, Alaska Earthquake: Version 2. R. D. Koehler and K. W. Franke, eds., Geotechnical Extreme Events Reconnaissance Association, [www.geerassociation.org](http://www.geerassociation.org), DOI: 10.18118/G6P07F.

Goughnour, R.R., and Pestana, J.M., 1998. Mechanical behavior of stone columns under seismic loading. *Proc., 2nd Int. Conf. Ground Improvement Techniques*, CI-Premier, Singapore, 157–162.

Green, R.A., Olgun, C.G., and Wissmann, K.J., 2008. Shear stress redistribution as a mechanism to mitigate the risk of liquefaction. *Geotechnical Earthquake Engineering and Soil Dynamics IV GSP 181*, ASCE, Reston, VA.

Gueguin, M., de Buhan, P., and Hassen, G., 2013. A homogenization approach for evaluating the longitudinal shear stiffness of reinforced soils: column versus cross trench configuration. *International Journal for Numerical and Analytical Methods in Geomechanics*, 37, 3150–3172.

Hasheminezhad, A., and Bahadori, H., 2019. Seismic response of shallow foundations over liquefiable soils improved by deep soil mixing columns. *Computers and Geotechnics*, 110(2019), 251–273.

Idriss, I.M., and Boulanger, R.W., 2008. Soil liquefaction during earthquakes. Monograph MNO-12, Earthquake Engineering Research Institute, Oakland, CA.

Ishii, I., Towhata, I., Hiradate, R., Tsukuni, S., Uchida, A., Sawada, S., and Yamauchi, T., 2017. Design of grid-wall soil improvement to mitigate soil liquefaction damage in residential areas of Urayasu. *Journal of Japanese Society of Civil Engineers*, 5, 27–44.

Ishikawa, A., Shamoto, Y., and Kimura, T., 2016. A simplified method for evaluating the liquefaction of sandy soil confined by lattice-type deep mixing wall. In *15th Asian Regional Conference on Soil Mechanics and Geotechnical Engineering*, Japanese Geotechnical Society Special Publication, 2153–2158, DOI: 10.3208/jgssp.JPN-017.

Ishikawa, A., and Asaka, Y., 2006. Seismic responses of column and grid-type improved grounds. *Proceedings of the International Conference on Physical Modelling in Geotechnics*, Taylor and Francis Group, London, UK, 521–526.

Itasca, 2016. *FLAC, Fast Lagrangian Analysis of Continua, User's Guide, Version 8.0*. Itasca Consulting Group, Inc., Minneapolis, MN.

Japanese Geotechnical Society, 1998. *Remedial measures against soil liquefaction: from investigation and design to implementation*. Taylor & Francis, New York, NY.

Khosravi, M., Boulanger, R.W., Wilson, D.W., Olgun, C.G., Tamura, S., and Wang, Y., 2017. Dynamic centrifuge tests of structures with shallow foundations on soft clay reinforced by soil-cement grids. *Soils and Foundations*, Japanese Geotechnical Society, 57(4), 501–513, DOI: 10.1016/j.sandf.2017.06.002.

Khosravi, M., Boulanger, R.W., Wilson, D.W., Olgun, C.G., Shao, L., and Tamura, S., 2019. Stress transfer from rocking shallow foundations on soil-cement reinforced clay. *Soils and Foundations*, Japanese Geotechnical Society, DOI: 10.1016/j.sandf.2019.04.003.

Khosravi, M., Pourakbar, M., Soroush, A., Zaregarizi, S., Hung, W.Y., and Nabizadeh, A., 2020. Dynamic centrifuge test of an embankment underlain by liquefiable soil and isolated soil-cement columns. *17<sup>th</sup> World Conference on Earthquake Engineering*, 17WCEE, Sendai, Japan, paper 4b-0037.

Kirby, R.C., Roussel, G.L., Barneich, J.A., Yiadom, A.B., and Todaro, S.M., 2010. Design and construction of seismic upgrades at San Pablo Dam using CDSM. *30th Annual USSD Conference*, United States Society on Dams, 137–151.

Kitazume, M., 2016. Applications of centrifuge modeling to liquefaction mitigation techniques. *Proceedings of Eurofuge 2016, 3<sup>rd</sup> European Conference on Physical Modelling in Geotechnics*, International Society of Soil Mechanics and Geotechnical Engineering.

Kitazume, M., Okano, K., and Miyajima, S., 2000. Centrifuge Model Tests on Failure Envelope of Column-Type DMM-Improved Ground, *Soils and Foundations*, 40(4), 43–55.

Kitazume, M., and Takahashi, H., 2010. Centrifuge model tests on effect of deep mixing wall spacing on liquefaction mitigation. Proc., 7th Int. Conf. on Urban Earthquake Engineering and 5th Int. Conf. on Earthquake Engineering, Tokyo Institute of Technology, Tokyo, 473–478.

Kitazume, M., and Terashi, M., 2013. *The Deep Mixing Method*. CRC Press/Balkema, Leiden, The Netherlands.

Koga, Y., Matsuo, O., Enokida, M., Ito, K., and Suzuki, Y., 1988. Shaking table test on DMM method as a countermeasure against liquefaction of sandy ground, (Part 2) Effects of improved ground in grid configuration against liquefaction. 23<sup>rd</sup> Japan National Conference on Soil Mechanics and Foundation Engineering, 1019–1020.

Koseki, J., 2018. Countermeasures against liquefaction. *Developments in Earthquake Geotechnics*, S. Iai, ed., Geotechnical, Geological, and Earthquake Engineering, Springer, 43, DOI: 10.1007/978-3-319-62069-5\_4.

Koseki, J., Tsutsumi, Y., Namikawa, T., Mihira, S., Salas-Monge, R., Sano, Y., and Nakajima, S., 2008. Shear and tensile properties of cement-treated sands and their application to liquefaction mitigation. Keynote Lecture. In: *Proceedings of 4th international symposium on deformation characteristics of geomaterials (IS-Atlanta 2008)*, 1, 27–50.

Mahboubi, A., and Ajorloo, A., 2005. Experimental study of the mechanical behavior of plastic concrete in triaxial compression. *Cement and Concrete Research*, 35(2005), 412–219.

Martin, J.R., Olgun, C.G., Mitchell, J.K., and Durgunoglu, H.T., 2004. High-modulus columns for liquefaction mitigation. *J. of Geotech. and Geoenviron. Eng.*, 130(6), 561–571.

Morikawa, Y., Takahashi, H., Wakaki, T., Okuno, N., Takahashi, N., and Towhata, I., 2015. Dynamic centrifuge model tests on pile-type deep mixing method reducing lateral flow of liquefied ground. *Proceedings, Deep Mixing 2015 Conference*, Deep Foundation Institute, 365–374.

Moseley, M.P., and Kirsch, K., 2004. *Ground improvement: 2<sup>nd</sup> edition*. Spon Press, Taylor & Francis Group, New York, NY.

Namikawa, T., Koseki, J., and Suzuki, Y., 2007. Finite element analysis of lattice-shaped ground improvement by cement-mixing for liquefaction mitigation. *Soils and Foundations*, 47(3), 559–76.

Navin, M.P., and Filz, G.M., 2006. *Simplified Reliability-Based Procedures for Design and Construction Quality Assurance of Foundations Improved by the Deep Mixing Method*, Federal Highway Administration, Washington, DC.

Nguyen, T.V., Rayamajhi, D., Boulanger, R.W., Ashford, S.A., Lu, J., Elgamal, A., and Shao, L., 2013. Design of DSM grids for liquefaction remediation. *Journal of Geotechnical and Geoenvironmental Engineering*, ASCE, 139(11), 1923–1933, DOI: 10.1061/(ASCE)GT.1943-5606.0000921.

Niina, A., Saitoh, S., Babasaki, R., Miyata, T., and Tanaka, K., 1981. Engineering properties of improved soil obtained by stabilizing alluvial clay from various regions with cement slurry. *Takenaka Technical Research Report*, 25, 1–21 (in Japanese).

Olgun, C.G., and Martin, J.R., 2008a. Numerical modeling of the seismic response of columnar reinforced ground. *Geotechnical Earthquake Engineering and Soil Dynamics IV GSP 181*, ASCE, Reston, VA.

Olgun, C.G., and Martin, J.R., 2008b. Effectiveness of jet-grout columns for mitigation of liquefaction during earthquakes. *Geotechnical Engineering for Disaster Mitigation and Rehabilitation*, Liu, Deng, and Chu, eds., Springer Link, 768–773.

O'Rourke, T.D., and Goh, S.H., 1997. Reduction of liquefaction hazards by deep soil mixing. NCEER/INCEDE Workshop, MCEER, Univ. at Buffalo, State Univ. of New York, Buffalo, NY.

Papadimitriou, A.G., Bouckovalas, G.D., Vytiniotis, A.C., and Bakas, G.J., 2006. Equivalence between 2D and 3D numerical simulations of the seismic response of improved sites. *Proc., 6th European Conf. on Numerical Methods in Geotechnical Engineering*, Taylor & Francis, London, 809–816.

PLAXIS (2016). R. B. J. Brinkgreve, S. Kumarswamy, and W. M. Swolfs (eds), P.O. Box 572, 2600 An Delft, Netherlands, ISBN-13: 978-90-76016-18-4.

Porbaha, A., Shibuya, S., and Kishida, T., 2000. State of the art in deep mixing technology. Part III: Geomaterial characterization. *Ground Improvement*, 4(3), 91–110.

PWRI, 1999. Design and Construction Manual of Countermeasures Against Liquefaction, Cooperative Research Reports of PWRI, 186 (in Japanese).

Quiroga, A.J., Muraleetharan, K.K., Cerato, A.B., and Miller, G.A., 2015. Stress-strain behavior of cement-improved clays. GSP No. 256, Proceedings (CDROM), IFCEE 2015: International Foundations Congress and Equipment Expo 2015, Geo-Institute, ASCE, San Antonio, Texas, March, 2328–2338.

Rostami, R., Hytiris, N., Mickovski, S.B., and Bhattacharya, S., 2018. Seismic risk management of piles in liquefiable soils stabilized with cementation or lattice structures. *Geotechnical Research*, ICE.

Rahmani, A., and Baez, J., 2020. New approach to determine composite shear wave velocity of improved ground sites. *Journal of Geotechnical and Geoenvironmental Engineering*, ASCE, 146(10), 06020017, DOI: 10.1061/(ASCE)GT.1943-5606.0002350.

Rayamajhi, D., Nguyen, T.V., Ashford, S.A., Boulanger, R.W., Lu, J., Elgamal, A., and Shao, L., 2014. Numerical study of shear stress distribution for discrete columns in liquefiable soils. *Journal of Geotechnical and Geoenvironmental Engineering*, ASCE, 140(3), 04013034, DOI: 10.1061/(ASCE)GT.1943-5606.0000970.

Rayamajhi, D., Tamura, S., Khosravi, M., Boulanger, R.W., Wilson, D.W., Ashford, S.A., and Olgun, C.G., 2015a. Dynamic centrifuge tests to evaluate reinforcing mechanisms of soil-cement columns in liquefiable sand. *Journal of Geotechnical and Geoenvironmental Engineering*, ASCE, 141(6), 04015015, DOI: 10.1061/(ASCE)GT.1943-5606.0001298.

Rayamajhi, D., Tamura, S., Khosravi, M., Boulanger, R.W., Wilson, D.W., Ashford, S.A., and Olgun, C.G., 2015b. Investigating reinforcing effects of soil-cement columns in liquefiable sand using dynamic centrifuge tests. *Proc. Deep Mixing 2015 Conf., Deep Foundations Institute*, Hawthorne, NJ, 375–384.

Rayamajhi, D., Ashford, S.A., Boulanger, R.W., and Elgamal, A., 2016. Dense granular columns in liquefiable ground: Shear reinforcement and cyclic stress ratio reduction. *Journal of Geotechnical and*

Geoenvironmental Engineering, ASCE, 142(7), 04016023, DOI: 0.1061/(ASCE)GT.1943-5606.0001474.

Seed, R.B., and Harder, L.F., 1990. SPT-Based Analysis of Cyclic Pore Pressure Generation and Undrained Residual Strength. H. Bolton Seed Memorial Symposium Proceedings, May 1990, Vol. 2, BiTech Publishers.

Stark, T.D., and Mesri, G., 1992. Undrained Shear Strength of Liquefied Sands for Stability Analysis. J. of Geotechnical Eng., ASCE, 118(11), 1727–1747.

Suzuki, K., Babasaki, R., and Suzuki, Y., 1991. Centrifuge tests on liquefaction-proof foundation. Proc., Centrifuge 91, Balkema, Rotterdam, Netherlands, 409–415.

Suzuki, Y., Saito, S., Onimura, S., Kimura, T., Uchida, A., and Okumura, R., 1996. Grid-shaped stabilized ground improved by deep cement mixing method against liquefaction for a building foundation. Tsuchi-to-Kiso, JGS, 44(3), 46–48 (in Japanese).

Takahashi, H., Kitazume, M., and Ishibashi, S., 2006. Effect of deep mixing wall spacing on liquefaction mitigation. Proceedings of the International Conference on Physical Modelling in Geotechnics 1, 585–590.

Takahashi, H., Morikawa, Y., Iba, H., Fukada, H., Maruyama, K., and Takehana, K., 2013. Experimental study on lattice-shaped cement treatment method for liquefaction countermeasure. Proc., 18<sup>th</sup> Intl. Conf. on Soil Mechanics and Geotechnical Engineering, Paris, 1619–1622.

Takahashi, H., Morikawa, Y., Takahashi, N., Takano, D., and Towhata, I., 2015. Effective plane arrangement of deep mixing piles to resist lateral flow of liquefied ground. Deep Foundations Institute, 121–130.

Takahashi, H., Takahashi, N., Morikawa, Y., Towhata, I., and Takano, D., 2016. Efficacy of pile-type improvement against lateral flow of liquefied ground. Geotechnique, 66(8), 617–26.

Tatsuoka, F., and Kobayashi, A., 1983. Triaxial strength characteristics of cement-treated soft clay. Proceedings of the 8th European Conference of SMFE, 421–426, Helsinki, Finland.

Terashi, M., Tanaka, H., Mitsumoto, T., Niidome, Y., and Honma, S., 1980. Fundamental properties of lime and cement treated soils (2nd Report). Report of the Port and Harbour Research Institute, 19(1), 33–62 (in Japanese).

Tokimatsu, K., Mizuno, H., and Kakurai, M., 1996. Building damage associated with geotechnical problems. Soils and Foundations, Special Issue on Geotechnical Aspects of the January 17 1995 Hyogoken-Nanbu Earthquake, 219–234.

Tokimatsu, K., and Asaka, Y., 1998. Effects of liquefaction induced ground displacements on pile performance in the 1995 Hyogoken-Nambu earthquake, Soils and Foundations, Special Issue, Japanese Geotechnical Society, 163–77.

Tokunaga, S., Kitazume, M., Morikawa, Y., Takahashi, H., Nagatsu, T., Honda, N., Onishi, T., Asanuma, T., Kubo, S., and Higashi, S., 2015. Performance of cement deep mixing method in 2011 Tohoku earthquake. Deep Foundations Institute, 1071–1080.

- Tong, B., Schaefer, V., Liu, Y., and Han, B., 2019. Optimization of deep mixing design for seismic liquefaction mitigation of caisson walls. *Geomatics, Natural Hazards and Risk*, 10(1), 287–313, DOI: 10.1080/19475705.2018.1521879.
- Topolnicki, M., 2004. Chapter 2: In situ soil mixing. In *Ground Improvement*, 2<sup>nd</sup> Edition. M. P. Moseley and K. Kirsch, eds., Spon Press, Taylor and Francis Group, New York.
- Tsukuni, S., Uchida, A., and Konishi, K., 2015. Effect of grid-form deep mixing wall to prevent liquefaction damage of small houses. *Proc., Deep Mixing 2015*, San Francisco, DFI, 781–800.
- Tsukuni, S., Ishii, I., Uchida, A., Imai, M., Yamauchi, T., and Ota, K., 2017. Design of grid-wall soil improvement to mitigate soil liquefaction damage in residential areas. 16<sup>th</sup> World Conference on Earthquake Engineering, 16WCEE, Santiago, Chile, paper 370.
- Uchida, A., Taya, Y., Honda, T., and Okumura, T., 2018. Effectiveness of simple method determining space for grid-form deep cement mixing walls. *Takenaka Technical Research Report No. 74*, Takenaka Research and Development Institute, Japan.
- Witthoeft, A.F., Warner, R.M., and Matasovic, N., 2019. Dynamic numerical evaluation of landfill perimeter levee on liquefiable subgrade mitigated with cement deep soil mixing. *Geo-Congress 2019, Geotechnical Special Publication 308*, ASCE, 151–159.
- Wooten, L., and Foreman, B., 2005. Deep soil mixing for seismic remediation of the Clemson upper and lower diversion dams. 25th Annual USSD Conference, United States Society on Dams.
- Yamasaki, K., Hemstreet, D., Gerondale, A., and Shao, L., 2015. Wet soil mixing for supporting bridge abutments on spread footings. *DFI Deep Mixing 2015*, San Francisco, California, 395–404.
- Yamashita, K., Shigeno, Y., Hamada, J., and Chang, D.-W., 2018. Seismic response analysis of piled raft with grid-form deep mixing walls under strong earthquakes with performance-based design concerns. *Soils and Foundations*, Elsevier, 58(2018), 65–84.
- Yamashita, K., Hamada, J., and Tanikawa, T., 2016. Static and seismic performance of a friction piled raft combined with deep mixing walls in soft ground. *Soils and Foundations*, 56(3), 559–573.
- Yang, Z., Elgamal, A., and Parra, E., 2003. Computational Model for Cyclic Mobility and Associated Shear Deformation. *J. Geotechnical and Geoenvironmental Engineering*, ASCE, 129(12), 1119–1127.
- Youd, T.L. et al. 2001. Liquefaction Resistance of Soils: Summary Report from the 1996 NCEER and 1998 NCEER/NSF Workshops on Evaluation of Liquefaction Resistance of Soils. *Journal of Geotechnical and Geoenvironmental Engineering*, ASCE, 127(4), 297–313.
- Yu, Y., Pu, J., and Ugai, K., 1997. Study of mechanical properties of soil cement mixture for a cutoff wall. *Soils and Foundations*, 37(4), 93–103.
- Zaregarizi, S., Khosravi, M., Coldwell, E., and Montgomery, J., 2021. Stochastic slope stability analysis of an embankment supported by isolated soil-cement columns considering spatial variability. *Journal of Geotechnical and Geoenvironmental Engineering*, ASCE, 147(4): 04021009, DOI: 10.1061/(ASCE)GT.1943-5606.0002488.

Ziotopoulou, K., and Boulanger, R.W., 2016. Plasticity modeling of liquefaction effects under sloping ground and irregular cyclic loading conditions. *Soil Dynamics and Earthquake Engineering*, 84(2016), 269–283, DOI: 10.1016/j.soildyn.2016.02.013.